Rhyacian magmatic arc rocks with sanukitoid geochemical signature from the Juiz de Fora Complex, Minas-Bahia Orogenic System (SE-Brazil)

Sandro Mauri[1]* , Monica Heilbron[2] , Henrique Bruno[2] , Rodson de Abreu Marques[3] , Carla Neto[1] , Cláudio de Morisson Valeriano[2] , Samuel Bersan[2] , Luiz Felipe Romero[1] , Mauro Cesar Geraldes[2]

Abstract

Sanukitoid rocks make up a complete magmatic series with distinct geochemical characteristics of TTG suites and granitoids from modern magmatic arcs and are regarded as markers of the transition from typically Archean geodynamics to modern plate tectonics. Although most known sanukitoid suites formed during the Neoarchean and Mesoarchean, numerous papers have characterized Paleoproterozoic magmatic arc granitoid rocks showing affinity with the sanukitoid series. This work presents new data from field, lithogeochemistry, zircon U-Pb geochronology, and Sm-Nd and Sr isotopic studies on granodioritic granulites with sanukitoid signatures from the Juiz de Fora Complex (JFC), one of the Paleoproterozoic tectonic components of the Minas-Bahia Orogenic System (MBOS), southern São Francisco Paleocontinent (southeastern Brazil). These rocks crystallized at ~2175 Ma and present values of εNd_t between −4.0 and +0.5, T_{DM} between 2.57 and 2.12 Ga, and $^{87}Sr/^{86}Sr_i$ between 0.6937 and 0.7137. We interpret these rocks as the result of crystallization of magmas from a hybrid mantle source extensively contaminated by crustal material during protracted subduction. In southeastern São Francisco Paleocontinent, the association of sanukitoid rocks with other magmatic arc rocks points to a complex and prolonged Rhyacian accretionary system similar to modern plate tectonics.

KEYWORDS: sanukitoid rocks; granodioritic granulites; zircon U-Pb geochronology; Sm-Nd and Sr isotopes; Rhyacian.

INTRODUCTION

The growth of continental masses throughout the Earth's history occurred through the addition of mantle-derived magma to the continental crust (Cawood *et al.* 2009, Niu and O'Hara 2009, Hawkesworth *et al.* 2010). Conditioned by global tectonic evolution, such magmatism gave rise to three principal products, namely the typical Archean tonalite-trondhjemite-granodiorite associations (TTG; Condie 2005, Martin *et al.* 2005, Moyen and Martin 2012, Laurent *et al.* 2014, Moyen and Laurent 2018), the modern basalt-andesite-dacite-rhyolite association (the BADR suites; Foley *et al.* 2002, Martin *et al.* 2010), and the sanukitoid rocks, a subordinate component, with chemical and isotopic characteristics distinct from TTG and BADR suites (Stern *et al.* 1989, Stern and Hanson 1991, Martin *et al.* 2005, 2010, Heilimo *et al.* 2010, Laurent *et al.* 2013, 2014).

The sanukitoid rocks make up a magmatic series that includes rocks of intermediate to acidic composition, high Sr, Ba, Ni, Cr, and MgO, high Mg#, high $(La/Yb)_N$, moderate to low Na_2O/K_2O ratios, and high enrichment in light rare earth elements (LREE) (Stern *et al.* 1989, Stern and Hanson 1991, Martin *et al.* 2005, 2010, Heilimo *et al.* 2010, Laurent *et al.* 2013, 2014). It is understood that sanukitoids were generated from the partial melting of peridotite mantle rocks that were previously enriched by the incorporation or addition of fluids or melts from subducted hydrated metabasaltic crust (Stern *et al.* 1989, Stern and Hanson 1991, Martin *et al.* 2010, Laurent *et al.* 2013, 2014, Semprich *et al.* 2015). In that context, these rocks have been interpreted as representing the transition from typical Archean geodynamics to Paleoproterozoic modern plate tectonics (Martin *et al.* 2005, 2010, Heilimo *et al.* 2010, Bruno *et al.* 2020). Although most of the known sanukitoid suites were formed in the Neoarchean and Mesoarchean (*e.g.*, Oliveira *et al.* 2009, 2010, Martin *et al.* 2010, Heilimo *et al.* 2010, Laurent *et al.* 2014, Sun *et al.* 2020, Valeriano *et al.* 2022), numerous works have characterized Proterozoic and Phanerozoic magmatic arc granitoid rocks with affinity with the sanukitoid series (*e.g.*, Fowler and Rollinson 2012, Seixas *et al.* 2013, Moreira *et al.* 2018, Bruno *et al.* 2020, 2021b, Raza *et al.* 2021, Zhang

[1]Programa de Pós-graduação em Geociências, Faculdade de Geologia, Universidade do Estado do Rio de Janeiro – Rio de Janeiro (RJ), Brazil. E-mails: sandromauriferreira@gmail.com, netocarla2@gmail.com, romerolipe@gmail.com

[2]Faculdade de Geologia, Universidade do Estado do Rio de Janeiro – Rio de Janeiro (RJ), Brazil. E-mails: monica.heilbron@gmail.com, henrique.bruno1602@gmail.com, mauro.geraldes@gmail.com, valeriano.claudio@gmail.com, samuelbersan@gmail.com

[3]Departamento de Geologia, Universidade Federal de Ouro Preto – Ouro Preto (MG), Brazil. E-mail: rodsonabreu@gmail.com

*Corresponding author.

et al. 2021). Therefore, the investigation of sanukitoid rocks has direct implications for a better understanding of when and how stable and long-lived subduction settings.

The southeastern region of Brazil records a complex geotectonic evolution involving the accretion and collage of several crustal terranes/blocks during at least two orogenic events: the Paleoproterozoic of the Minas-Bahia Orogenic System (MBOS), culminating with the formation of the São Francisco Paleocontinent (Heilbron *et al.* 2010, 2017, Alkmim and Teixeira 2017, Degler *et al.* 2018, Bruno *et al.* 2020, 2021a, 2021b); and the Neoproterozoic Brasiliano/Pan-African orogenies that resulted in the amalgamation of the Western Gondwana (Pedrosa-Soares *et al.* 2001, Noce *et al.* 2007, Tupinambá *et al.* 2012, Heilbron *et al.* 2017, 2020a, 2020b, Caxito *et al.* 2022). The Brasiliano orogenic event reworked the margins of the São Francisco Paleocontinent and was responsible for the inversion of Mesoproterozoic to Neoproterozoic sedimentary basins and the generation of widespread pre-, syn-, late-, and post-collisional magmatic suites (Heilbron *et al.* 2010, 2020a). Thus, the preserved regional structure is complex, with Paleoproterozoic basement inliers (*e.g.*, Juiz de Fora and Mantiqueira complexes), tectonically juxtaposed with Neoproterozoic supracrustal units (*e.g.*, Raposos/Andrelândia Group; Paciullo *et al.* 2000, Heilbron *et al.* 2020a), both metamorphosed up to granulite facies and intruded by multiple Brasiliano granitoid rocks (Heilbron *et al.* 2010, 2017, 2020a, 2020b).
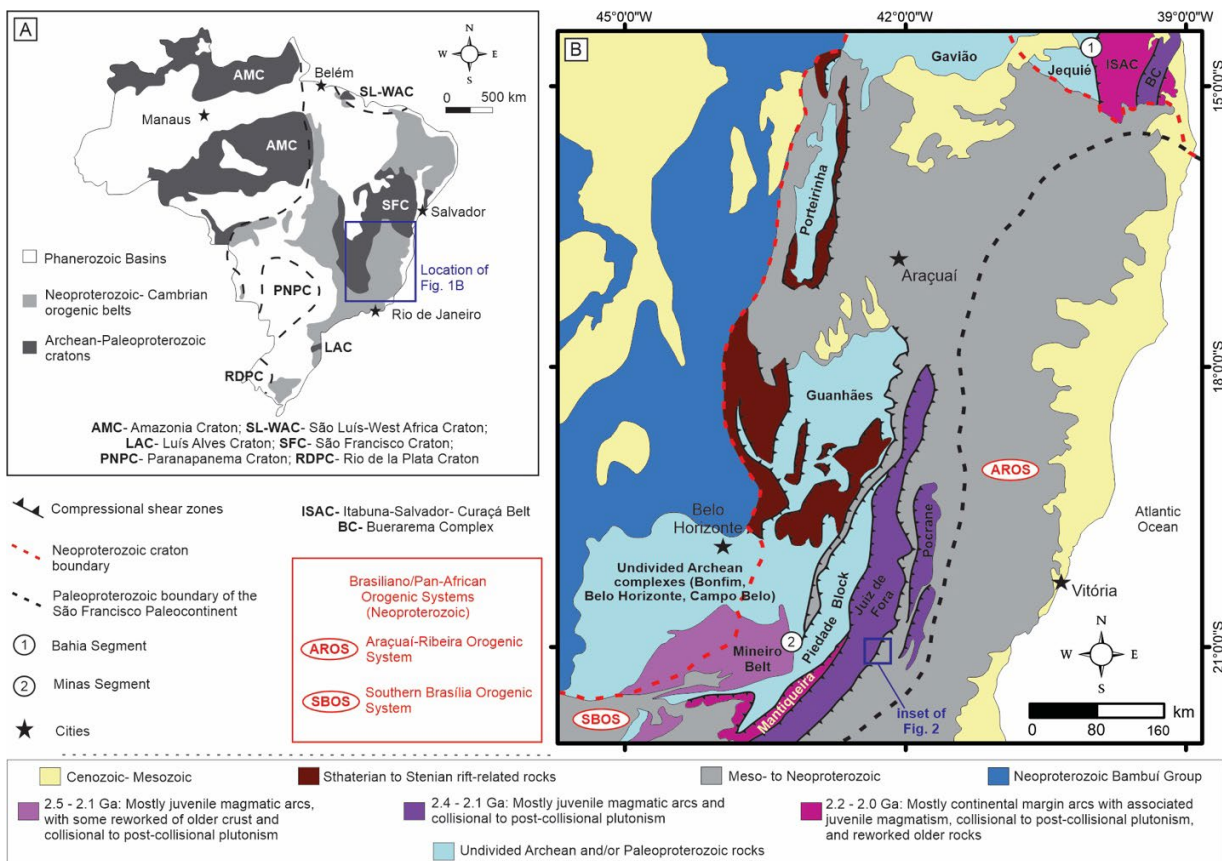
The Juiz de Fora Complex (JFC) comprises granitoid rocks metamorphosed under granulite facies with a wide compositional variation, which are interpreted to have been formed in an intraoceanic magmatic arc environment during the Siderian (Duarte *et al.* 1997, 2000, Heilbron *et al.* 1998, 2010, 2013, Degler *et al.* 2018, Araújo *et al.* 2021), with isotopic evidence of Mesoarchean crust reworking (Almeida *et al.* 2022). The JFC rocks were agglutinated along with the other components of the MBOS during the formation of the São Francisco Paleocontinent during the early Orosirian and were intensively reworked during the Neoproterozoic by the Brasiliano/Pan-African orogeny (Heilbron *et al.* 2010, 2017, Alkmim and Teixeira 2017, Araújo *et al.* 2021, Almeida *et al.* 2022). Considering that the JFC has ca. 400 km in length, the present work focuses on its northern segment. Combining Sm-Nd and Sr isotopes, together with whole-rock geochemistry, petrography, and field observations, magmatic arc rocks with sanukitoid signatures were characterized, and their ages were determined by U-Pb geochronology. The new data are compared with a compilation of other Paleoproterozoic sanukitoid suites from the southern Brazil, which allowed important insights regarding the petrogenesis of sanukitoid rocks and the geodynamic evolution of the São Francisco Paleocontinent.

TECTONIC FRAMEWORK

The São Francisco Paleocontinent

The São Francisco Paleocontinent is the precursor of the present São Francisco Craton, cropping out in the southeastern and northeastern regions of Brazil (Fig. 1A). It was agglutinated

Figure 1. Tectonic framework of the São Francisco Paleocontinent: (A) Geological compartments of Brazil (modified from Heilbron *et al.* 2017) and (B) Archean blocks and Paleoproterozoic magmatic arcs of the Minas-Bahia Orogenic System in the São Francisco Paleocontinent (modified from Alkmim and Teixeira 2017, Barbosa and Barbosa 2017, Degler *et al.* 2018, Bersan *et al.* 2020, Bruno *et al.* 2021b).

from the collage of several Archean crustal blocks (*e.g.*, Gavião, Jequié, Piedade, Belo Horizonte, and Bonfim) during the Paleoproterozoic, with the formation of several orogenic belts (such as the MBOS) during the Siderian and Orosirian periods (Fig. 1B; Teixeira *et al.* 2015, 2017, Alkmim and Teixeira 2017, Barbosa and Barbosa 2017). During the development of the Neoproterozoic Brasiliano/Pan-African orogenic system, the São Francisco Paleocontinent had its margins variably reworked (Fig. 1B). Some of its constituents, such as the JFC, the Guanhães Block, and the Mantiqueira Complex, crop out as reworked inliers within the Neoproterozoic orogens (Heilbron *et al.* 1998, 2010, Silva *et al.* 2002, Noce *et al.* 2007, Novo *et al.* 2011, Degler *et al.* 2018, Araújo *et al.* 2021, Grochowski *et al.* 2021, Almeida *et al.* 2022). This Paleoproterozoic orogenic system is preserved in two sectors of the São Francisco Craton: one to the north, in Bahia state (the Bahia Segment), and the other one to further south, in Minas Gerais state (the Minas Segment of the MBOS; Fig. 1B).

In the southernmost sector of the São Francisco Paleocontinent, Archean blocks are bounded by Siderian-Rhyacian-Orosirian orogenic belts in the Minas Segment of the MBOS (Ávila *et al.* 2010, 2014, Seixas *et al.* 2013, Barbosa *et al.* 2015, Teixeira *et al.* 2015, 2017, Alkmim and Teixeira 2017, Moreira *et al.* 2018, Bruno *et al.* 2020, 2021a, 2021b). The Archean exposures are represented by greenstone belt remnants (Pimhuí, Rio das Velhas, and Pitangui) and several metamorphic complexes (*e.g.*, Bonfim, Belo Horizonte, Campo Belo, and Piedade complexes) comprising gneisses, migmatites, and granitoid rocks. These crustal complexes/blocks acquired stability by the late-Neoarchean, establishing the core of the São Francisco Paleocontinent, which was further amalgamated with other Archean blocks (Piedade and others) between the Siderian and Early Orosirian, resulting in the formation of the Minas segment of the MBOS (Barbosa *et al.* 2015, Teixeira *et al.* 2015, 2017, Alkmim and Teixeira 2017, Bruno *et al.* 2020, 2021b).

The Minas Segment of the MBOS

The Minas segment comprises the Mineiro Belt and the Mantiqueira and Juiz de Fora complexes. The Mineiro Belt, with TTG suites, sanukitoid and granitoid rocks, diorites, gabbros, and supracrustal sequences, corresponds to juvenile to

mature magmatic arcs built between 2.45 and 2.10 Ga, resulting from the westward accretion of the Piedade Block to the core of the São Francisco Paleocontinent (Fig. 1B; Noce *et al.* 2000, Ávila *et al.* 2010, 2014, Barbosa *et al.* 2015, Seixas *et al.* 2012, 2013, Teixeira *et al.* 2015, 2017, Alkmim and Teixeira 2017, Moreira *et al.* 2018, Bruno *et al.* 2020, 2021b).

To the east of the Piedade Block, the Mantiqueira Complex comprises TTG suites and biotite-hornblende gneisses with continental to mantle-derived signatures. They were intruded by late to post-collisional basic rocks (Duarte *et al.* 2004, Teixeira *et al.* 2017, Bruno *et al.* 2020). The Mantiqueira Complex has been interpreted as a reworked Archean microcontinent accreted to the Piedade Block between 2.10 and 2.00 Ga, and reworked during the Neoproterozoic as a result of the development of the Araçuaí-Ribeira Orogenic System (Duarte *et al.* 2004, Noce *et al.* 2007, Heilbron *et al.* 2010, Degler *et al.* 2018, Kuribara *et al.* 2019, Cutts *et al.* 2020, Bruno *et al.* 2020, 2021a, 2021b).

The Juiz de Fora Complex

The JFC orthogranulites protoliths comprise magmatic arc calc-alkaline granitoid rocks, TTG, and sanukitoid suites, associated with mafic rocks of different geochemical signatures (mid-oceanic ridge basalt [MORB], island arc tholeiite [IAT], and post-collision alkaline basalts) with crystallization ages ranging from 2.40 to 1.90 Ga (Table 1; Heilbron *et al.* 1998, 2010, 2013, Silva *et al.* 2002, André *et al.* 2009, Degler *et al.* 2018, Araújo *et al.* 2019, 2021, Kuribara *et al.* 2019, Almeida *et al.* 2022, Faria *et al.* 2022). While previous works have interpreted the JFC as an initially juvenile intraoceanic magmatic arc that evolved into a more mature one (Duarte *et al.* 1997, 2000, Heilbron *et al.* 1998, 2010, 2013, Araújo *et al.* 2019, 2021), recent works have shown some evidence of reworking of some older Mesoarchean crust within this complex (Araújo *et al.* 2021, Almeida *et al.* 2022). The JFC represents the last magmatic arc to be accreted onto the southern margin of the São Francisco Paleocontinent, having collided with the Mantiqueira Complex during the early Orosirian (between 2.03 and 2.02 Ga; Heilbron *et al.* 1998, 2010, Noce *et al.* 2007, Degler *et al.* 2018, Araújo *et al.* 2019, 2021, Bruno *et al.* 2020, 2021a, 2021b, Almeida *et al.* 2022).

Previous tectonic models for the evolution of the JFC suggest an early evolutionary stage with moderately juvenile

Table 1. Compilation of Juiz de Fora Complex zircon U-Pb geochronology data.

Sample	Lithotype	Tectonic classification	Method	Age (Ma)			References
				Inherited	Magmatic	Metamorphic	
5B	Felsic granulite	-	TIMS	-	2134	579	Machado *et al.* (1996)
LC-17	Enderbitic granulite	-	SHRIMP	-	2985 ± 17	808 ± 360	Silva *et al.* (2002)
LC-17	Enderbitic granulite	-	SHRIMP	-	2985 ± 17	2856 ± 10	Silva *et al.* (2002)
LC-32	Charnokitic granulite	-	SHRIMP	-	2195 ± 15	587 ± 9	Silva *et al.* (2002)
1070	Mafic granulite	E-MORB	LA-MC-ICP-MS		2427 ± 9	654 ± 12	Heilbron *et al.* (2010)
1076	Enderbitic granulite	-	LA-MC-ICP-MS		1966 ± 38	587 ± 15	Heilbron *et al.* (2010)

Table 1. Continuation.

Sample	Lithotype	Tectonic classification	Method	Age (Ma)			References
				Inherited	Magmatic	Metamorphic	
1065	Charnokitic granulite	-	LA-MC-ICP-MS		2199 ± 17	633 ± 140	Heilbron *et al.* (2010)
CJE-44	Mafic granulite	-	LA-MC-ICP-MS		1765 ± 34	586 ± 14	Heilbron *et al.* (2010)
1062	Charno-enderbitic granulite	-	LA-MC-ICP-MS		1656 ± 69	590 ± 5	Heilbron *et al.* (2010)
LC-66	Norite	-	SHRIMP		2119 ± 16	579 ± 5	Noce *et al.* (2007)
UB-1	Enderbite	-	SHRIMP		2084 ± 13	594 ± 37	Noce *et al.* (2007)
IV-48	Granodioritic orthogneiss	-	SHRIMP		2107 ± 71	580 ± 19	Degler *et al.* (2018)
M-03	Tonalitic orthogneiss	-	LA-MC-ICP-MS		2110 ± 12	-	Degler *et al.* (2018)
LC-07	Tonalitic orthogneiss	-	SHRIMP		2122 ± 11	565 ± 7	Degler *et al.* (2018)
RC-101	Enderbitic orthogneiss	-	SHRIMP		2144 ± 13	-	Degler *et al.* (2018)
RC-103	Enderbitic orthogneiss	-	SHRIMP		2143 ± 21	-	Degler *et al.* (2018)
VA-LM-07B	Enderbitic granulite	Low-K tholeiite	SHRIMP	-	2446 ± 10	-	Araújo *et al.* (2019, 2021)
RP-LM-04	Charnokitic granulite	Sanukitoid	SHRIMP	-	2182 ± 13	561 ± 41	Araújo *et al.* (2019, 2021)
RP-LM-04	Charnokitic granulite	Sanukitoid	SHRIMP		2182 ± 13	2021 ± 29	Araújo *et al.* (2019, 2021)
BP-LM-13	Charno-enderbitic granulite	Sanukitoid	SHRIMP	-	2200 ± 7	-	Araújo *et al.* (2019, 2021)
BP-LM-12	Charno-enderbitic granulite	TTG	SHRIMP	2364 ± 16	2197 ± 13	588 ± 18	Araújo *et al.* (2019, 2021)
BP-CM-151	Mafic orthogranulite	Tholeiite	LA-MC-ICP-MS	2395 ± 19	2134 ± 43	544 ± 19	Araújo *et al.* (2019, 2021)
RB13A	Charnokite	-	LA-MC-ICP-MS	-	2039 ± 22	589 ± 6	Kuribara *et al.* (2019)
MAJF26	Enderbitic orthogranulite	TTG	LA-ICP-MS	2380 ± 19	2085 ± 24	591 ± 10	Almeida *et al.* (2022)
CTVC 8D	Mafic orthogranulite	IAT	LA-ICP-MS	-	2101 ± 12	-	Almeida *et al.* (2022)
ADVC 241A	Enderbitic orthogranulite	Sanukitoid	LA-ICP-MS	-	2067 ± 6	-	Almeida *et al.* (2022)
SJVC 72A	Mafic orthogranulite	E-MORB	LA-ICP-MS	-	2038 ± 5	512 ± 11	Almeida *et al.* (2022)
MRVC 23A	Charnokitic orthogranulite	Hybrid granitoid	LA-ICP-MS	-	2019 ± 16	636 ± 39	Almeida *et al.* (2022)
MAJF 14	Charno-enderbitic granulite	Hybrid granitoid	LA-ICP-MS	2730 ± 19	1982 ± 18	600 ± 41	Almeida *et al.* (2022)
CPR-03	Granulitic orthogneiss	-	LA-MC-ICP-MS	-	2209 ± 22	596 ± 20	Faria *et al.* (2022)
CPR-04	Granulitic orthogneiss	-	LA-MC-ICP-MS	-	2199 ± 21	603 ± 20	Faria *et al.* (2022)
CPR-08	Granulitic orthogneiss	-	LA-MC-ICP-MS	-	2104 ± 16	622 ± 46	Faria *et al.* (2022)
CPR-10	Granulitic orthogneiss	-	LA-MC-ICP-MS	-	2196 ± 14	633 ± 22	Faria *et al.* (2022)
CPR-13	Migmatitic orthogneiss	-	LA-MC-ICP-MS	-	2176 ± 26	600 ± 18	Faria *et al.* (2022)
CPR-18	Migmatitic orthogneiss	-	LA-MC-ICP-MS	-	2160 ± 39	584 ± 29	Faria *et al.* (2022)
CPR-20	Migmatitic orthogneiss	-	LA-MC-ICP-MS	-	2121 ± 18	596 ± 16	Faria *et al.* (2022)

tholeiitic magmatism at 2.44 Ga, followed by moderately juvenile to evolved TTG-sanukitoid magmatic pulses between 2.20–2.18 and 2.07 Ga, and moderately juvenile tholeiitic magmatic pulses at 2.13 Ga (Araújo *et al.* 2019, 2021, Almeida *et al.* 2022). The JFC rocks record two high-grade metamorphic events: one in the beginning of the Orosirian (~2.03–2.02 Ga), interpreted as resulting from the collision of the JFC with the Mantiqueira Complex during the terminal phases of the São Francisco Paleocontinent amalgamation (Araújo *et al.* 2021), and another one in the Ediacaran (around 600–580 Ma), interpreted as the reworking of the continental margin by the Brasiliano/Pan-African orogenic system (Machado *et al.* 1996, Heilbron *et al.* 1998, 2010, 2020a, Kuribara *et al.* 2019, Cutts *et al.* 2020, Araújo *et al.* 2021, Almeida *et al.* 2022, Faria *et al.* 2022).

MATERIALS AND METHODS

The development of the present work involved field survey, petrographic descriptions, lithogeochemical analyses, whole-rock Sm-Nd and Sr isotopic analyses, and zircon U-Pb geochronology by a laser ablation multi-collector inductively coupled plasma source mass spectrometer (LA-MC-ICP-MS). Seven samples were pulverized at the Laboratório Geológico de Preparação de Amostras (LGPA/UERJ) and sent to Activation Laboratories Ltd. (Actlabs, Ancaster, Canada) for lithogeochemical analyses. For the Sm-Nd and Sr whole-rock isotope analysis, four samples were pulverized in the LGPA (UERJ) and sent to the Laboratório de Geocronologia e Isótopos Radiogênicos (LAGIR/UERJ), where the chemical separation of Sm, Nd, and Sr was carried out in cleanrooms and measurement of isotopic ratios was performed using a TRITON (Thermo Scientific) thermal ionization mass spectrometer (TIMS). For zircon U-Pb geochronology, two samples were analyzed at the Laboratório Multiusuário de Meio Ambiente e Materiais (MultiLab/UERJ) with an LA-MC-ICP-MS Neptune Plus mass spectrometer. Further details of the sample preparation routine, the analytical techniques, and equipment used, as well as the treatment of lithogeochemistry, Sm-Nd and Sr isotopes, and zircon U-Pb geochronology data, are provided in Supplementary Material A.

RESULTS

Field relationships and petrography

The JFC Paleoproterozoic rocks occur in razed anticline cores and as thrust slices interleaved with Neoproterozoic paragneiss and migmatitic paragneisses from the Raposos/Andrelândia Group and Neoproterozoic anatectic I-type granitoids from the Salvaterra Suite (Fig. 2). The contacts between JFC rocks and Neoproterozoic units are tectonic (faults, thrust zones, and shear zones). The main metamorphic foliation has an NNE-SSW strike and moderate to steep dips toward SE, and its distribution reflects large regional folds with vergence to W or NW (refer to geological cross section in Fig. 2).

The rocks of the JFC are granodioritic granulites ranging from bluish-gray to deep gray color (Figs. 3A-3C) and display medium grain size with predominant granoblastic (Fig. 3B)

and subordinate nematoblastic textures defined by oriented orthopyroxene grains (Fig. 3D). Millimeter to centimeter compositional banding characterized by light and dark gray tones is locally observed (Fig. 3A). The main mineralogy of the rocks is defined by plagioclase (34–55%), quartz (9–29%), K-feldspar (9–28%), and orthopyroxene (8–14%). Biotite (4–7%) occurs as either main or accessory phase. Clinopyroxene (0–3%), opaque minerals (0–2%), apatite (< 0.1%), zircon (< 0.2%), and titanite (0–0.1%) constitute the accessory phases.

Orthopyroxene crystals are xenoblastic (Fig. 3B) and often surrounded by retrometamorphic hornblende and biotite (Fig. 3F). Plagioclase (without twinning) occurs as equigranular aggregates, whereas K-feldspar crystals are microperthitic and quartz usually shows amoeboid to interlobed contacts. Myrmekitic intergrowth of quartz between plagioclase and K-feldspar (Fig. 3E) is a common feature. Sub-idioblastic to idioblastic biotite flake aggregates without preferential orientation (decussate texture) are also observed.

Two distinct mineral parageneses can be distinguished: one with plagioclase + quartz + K-feldspar + orthopyroxene ± clinopyroxene + opaque minerals ± titanite, with metamorphic peak characteristics and another with hornblende + biotite, of retrometamorphic origin, partially replacing orthopyroxene, clinopyroxene, and opaque minerals.
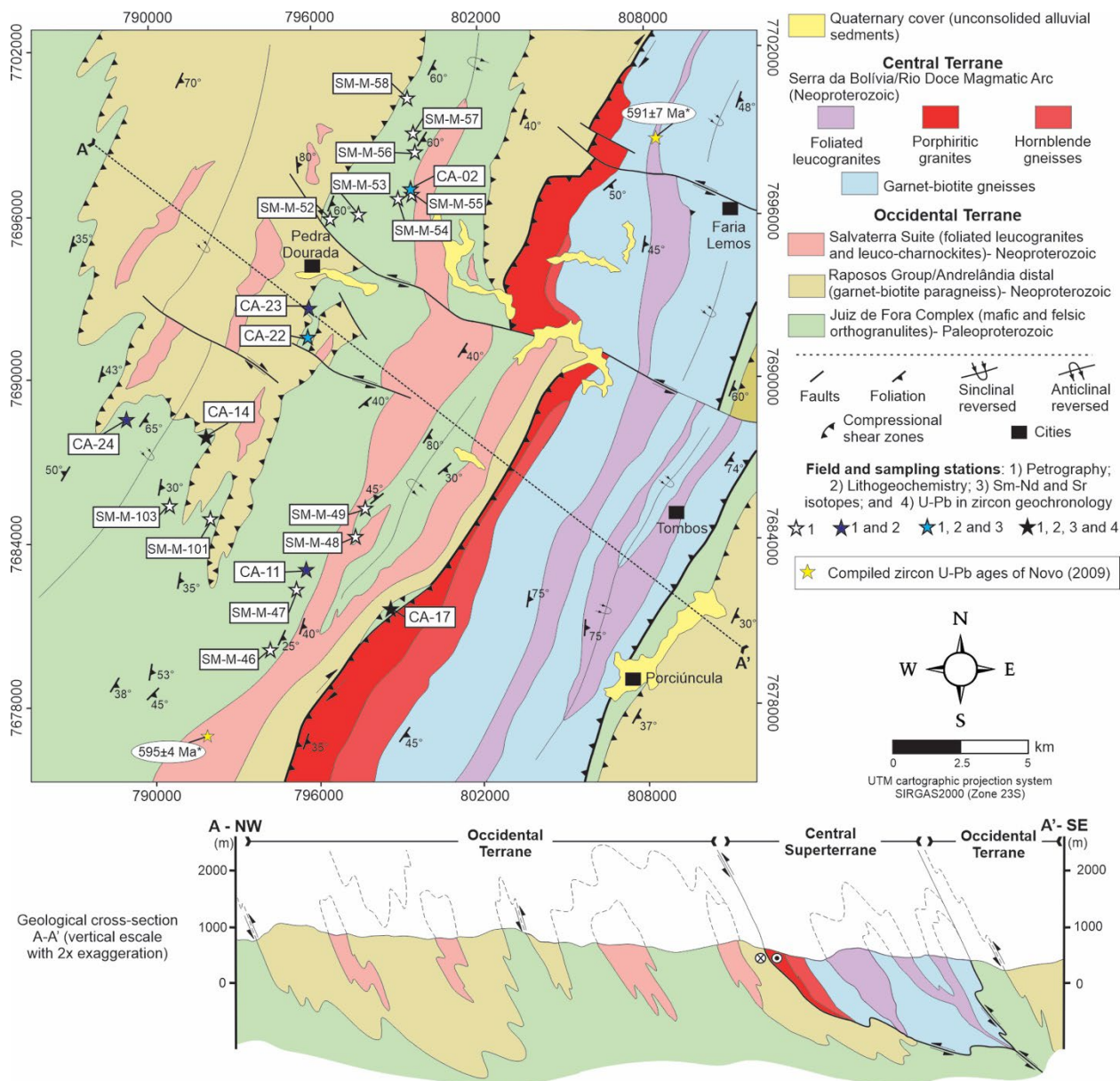
Whole-rock geochemistry

The whole-rock lithogeochemical data (Suppl. Mat. B) obtained for seven granodioritic granulites show that the investigated samples share many compositional affinities, allowing their characterization as a single igneous suite. They display intermediate SiO_2 contents (58.4 to 65.8 wt.%), moderate to high Mg# values (0.44 to 0.54), and plot in the diorite-granodiorite fields of the TAS diagram (Fig. 4A). The granodioritic granulites are calcic, calc-alkaline, and alkali-calcic (Fig. 4B) and share a typical magnesian and dominantly metaluminous affinity, with A/CNK ratios between 0.81 and 1.01 (Figs. 4C and 4D). They also have moderate to high Ba (between 489 and 1,389 ppm) and Sr (377 to 624 ppm) contents (Fig. 4E). Other important geochemical characteristics are the Na_2O/K_2O ratios between 0.71 and 2.34 and Cr and Ni contents between 40–110 ppm and < 50 ppm, respectively. In the ternary diagrams proposed by Laurent *et al.* (2014), the samples plot in the sanukitoid and high-K mafic sources fields (Figs. 4F and 4G).

The chondrite-normalized REE diagrams (Fig. 5A) show moderate fractionation between light and heavy REE, with $(La/Yb)_N$ ratios ranging between 9.55 and 15.15. Eu anomalies are absent to weakly negative or positive. In the primitive mantle normalized diagrams (Fig. 5B), the samples show enrichment of Ba, K, Pb, Nd, and Dy, as well as depletion of Th, Nb, P, Zr, and Ti.

Zircon U-Pb geochronology data

Zircon grains from samples CA-14 and CA-17 were analyzed by LA-MC-ICP-MS U-Pb techniques. The morphology and internal textures of the grains are shown in Fig. 6. The full analytical data set is shown in Suppl. Mat. B. The relationship between the U-Pb ages and Th/U ratios

Figure 2. Map and geological section of the study area, with field stations and sampling locations for lithogeochemistry, Sm-Nd and Sr isotopes, and U-Pb geochronology data.

Source: integration of regional geological maps (Carangola quadrangle, Noce *et al.* 2009), Novo (2009), and authors' data.

obtained for the different textural domains identified in the zircon grains for each of the analyzed samples is presented in Table 2.

Zircon grains from sample CA-14 are colorless and transparent, and display euhedral and subordinately subhedral morphology. They are mostly prismatic with pyramidal or rounded tips. Grain size ranges from 190 to 350 μm in length with dominant aspect ratios of 3:1, although the ratios of 4:1 and 2:1 are also observed. In the cathodoluminescence (CL) images, most grains show two distinct domains highly luminescent cores, with strong oscillatory zoning, and more homogeneous rims, with weak to no oscillatory zoning (Fig. 6A). The boundary between cores and rims is usually abrupt, with truncation of the oscillatory zoning pattern by the rim, suggesting processes of grain corrosion followed by metamorphic overgrowth. A total of 36 analyses in cores and rims were performed in thirty-two zircon grains, avoiding metamictic crystals and grains with inclusions and fractures. From the analyzed grains, 16 spot data were

rejected because of high common Pb contents and/or large uncertainties of their isotopic ratios. Data from 20 spots define a discordia with an upper intercept age of 2176±7 Ma (MSWD = 1.3), interpreted as magmatic crystallization age, and a lower intercept at 581±12 Ma, interpreted to reflect the age of metamorphic overprint (Figs. 6B and Table 2).

In sample CA-17, the zircon grains are predominantly subhedral to euhedral, prismatic with a pyramidal to rounded tips, and also colorless and transparent. Inclusions, although not very abundant, are also observed. Zircon grains have lengths ranging between 210 and 360 μm and aspect ratios of 3:1 and 4:1, with subordinate ratios of 2:1 and 3:2. CL textures are relatively complex. Most of the grains exhibit strongly luminescent cores with oscillatory zoning (typical of igneous zircons) surrounded by more homogeneous and weakly zoned rims (Fig. 6C). As in the previous sample, the boundary between these two domains is commonly abrupt. A total of 36 analyses in cores and rims were performed in twenty-seven zircon grains.
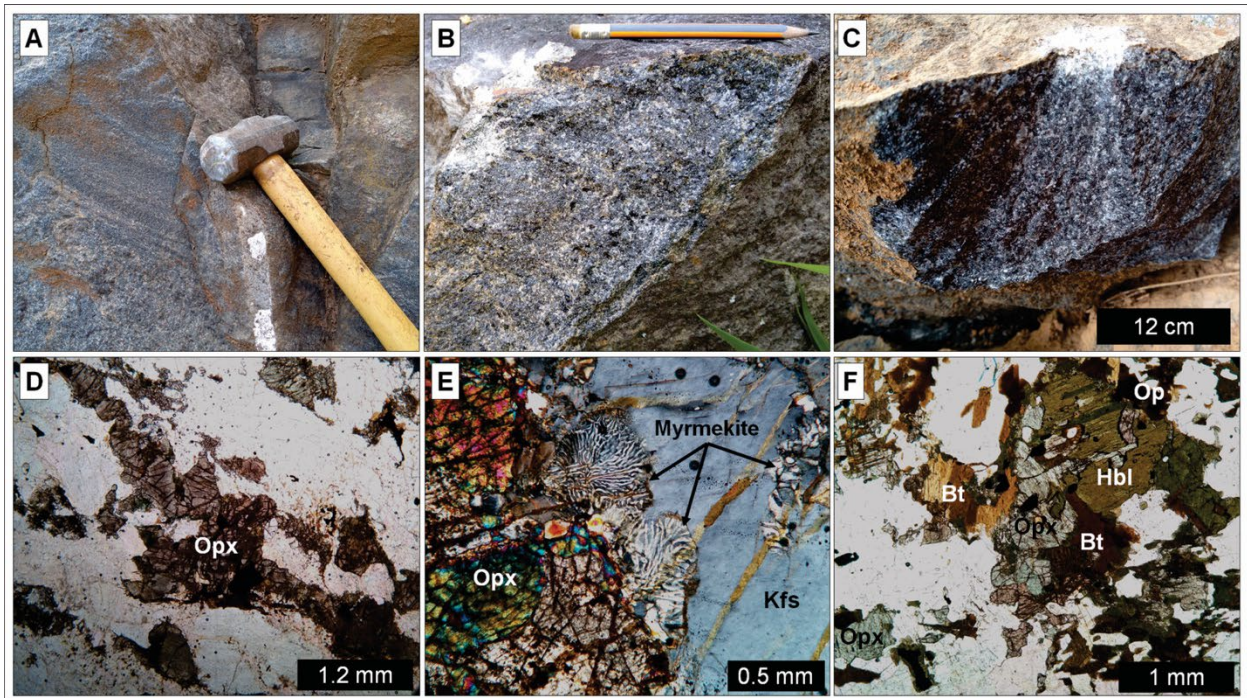
Figure 3. Field and petrographic aspects of the Juiz de Fora Complex granodioritic granulites in the Pedra Dourada region (MG): (A) compositional banding of light gray and medium grey granodioritic granulites; (B) detail of the granodioritic granulite with pyroxene porphyroblasts (dark spots); (C) detail of a dark gray granulite; (D) photomicrograph in plane-polarized light showing nematoblastic texture with oriented orthopyroxene (Opx) grains; (E) photomicrograph in cross-polarized light showing myrmekite within K-feldspar (Kfs) and Plagioclase (Pl) crystals; and (F) photomicrograph in plane-polarized light showing orthopyroxene (Opx) and opaque minerals (Op) grains partially replaced by retrometamorphic hornblende (Hbl) and biotite (Bt).
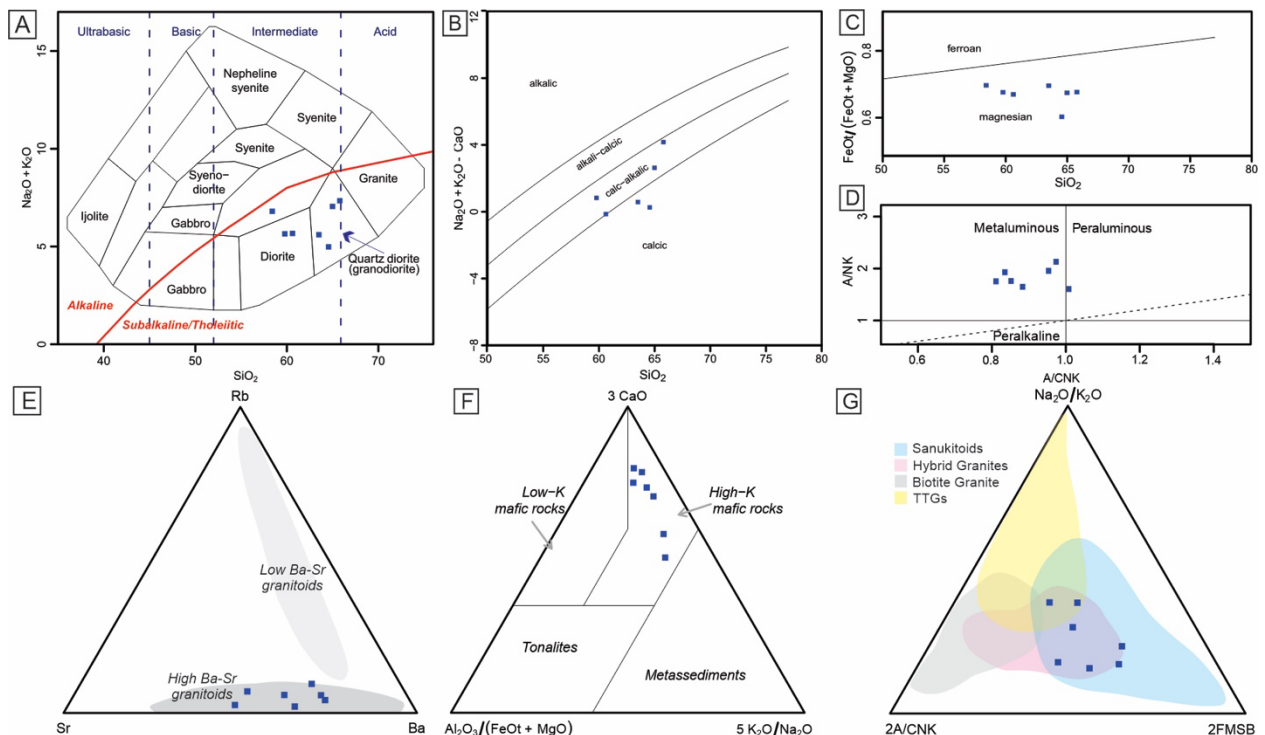
Figure 4. Lithogeochemical classification diagrams and tectonic setting for the Juiz de Fora Complex granodioritic granulites: (A) TAS diagram by Cox *et al.* (1979); (B) $Na_2O + K_2O + CaO$ vs. SiO_2 diagram from Frost *et al.* (2001); (C) $FeO_t/(FeO_t + MgO)$ vs. SiO_2 diagram by Frost *et al.* (2001); (D) A/NK vs. A/CNK diagram by Shand (1943); (E) triangular diagram Rb-Ba-Sr with the field for high Ba-Sr granites from Tarney and Jones (1994); (F) source diagram by Laurent *et al.* (2014); (G) ternary classification diagram for late-Archean granitoids by Laurent *et al.* (2014).

Notably, 21 spots were discarded using the same criteria described for sample CA-14. The data from 15 spots were used to construct a discordia with upper intercept age of 2175 ± 12 Ma (MSWD = 2.4) and lower intercept age of 605 ± 26 Ma, interpreted, respectively, as the magmatic crystallization and as the metamorphic ages (Fig. 6D and Table 2).
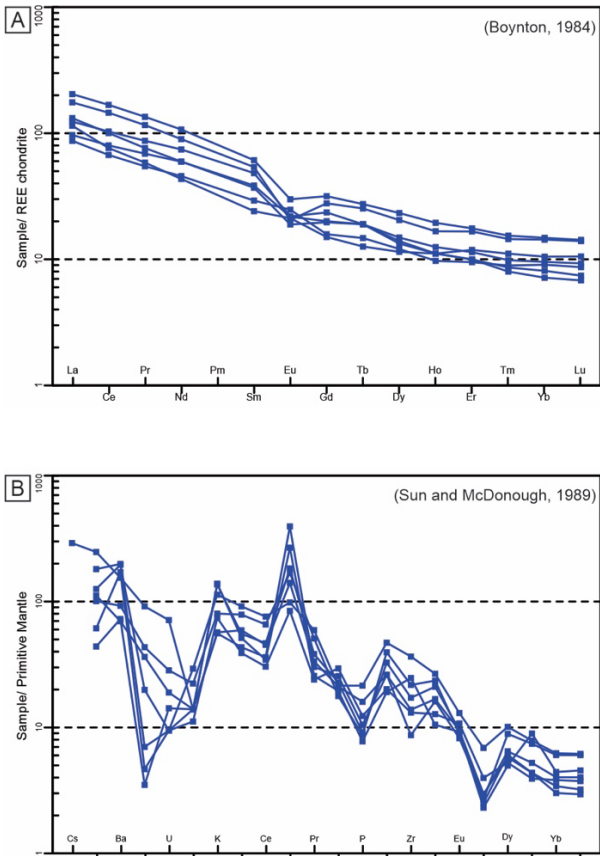
Figure 5. REE patterns for the Juiz de Fora Complex granodioritic granulites: (A) chondrite-normalized to REE diagrams (Boynton 1984) and (B) primitive mantle-normalized REE diagrams (Sun and McDonough 1989).

Sm-Nd and Sr isotopes

Four samples were selected for the determination of ID-TIMS Sm-Nd and natural Sr isotopic compositions (Table 3). The Nd and Sr isotope ratios were calculated to initial values according to the U-Pb crystallization ages obtained from samples CA-14 and CA-17 (2176 and 2175 Ma, respectively).

Sample CA-02 has the most negative initial εNd (-4.0) and the oldest T_{DM} (2.57 Ga). Samples CA-14, CA-17, and CA-22, in turn, present the initial near-CHUR εNd values, between -1.2 and 0.5, as well as T_{DM} ages between 2.30 and 2.12 Ga, which are near or even coincident with the age of magmatic crystallization. The obtained initial $^{87}Sr/^{86}Sr$ ratios range from 0.6937 to 0.7137 (Table 3).

DISCUSSION

Petrogenetic implications

The geochemical data strongly suggest that these rocks were generated in a magmatic arc setting: intermediate SiO_2 contents, affinity with the calc-alkaline series, magnesian and metaluminous to weakly peraluminous character, moderate to high Ba, Sr, and LILE contents and low HFSE contents, moderate $(La/Yb)_N$ ratios, and significantly fractionation between LREE and HREE, with slightly positive or negative to absent Eu anomalies (Hawkesworth *et al.* 1994, Foley *et al.* 2002, Rustioni *et al.* 2021). Depletion in Nb and Ti together with Pb enrichment is also the main characteristics of modern
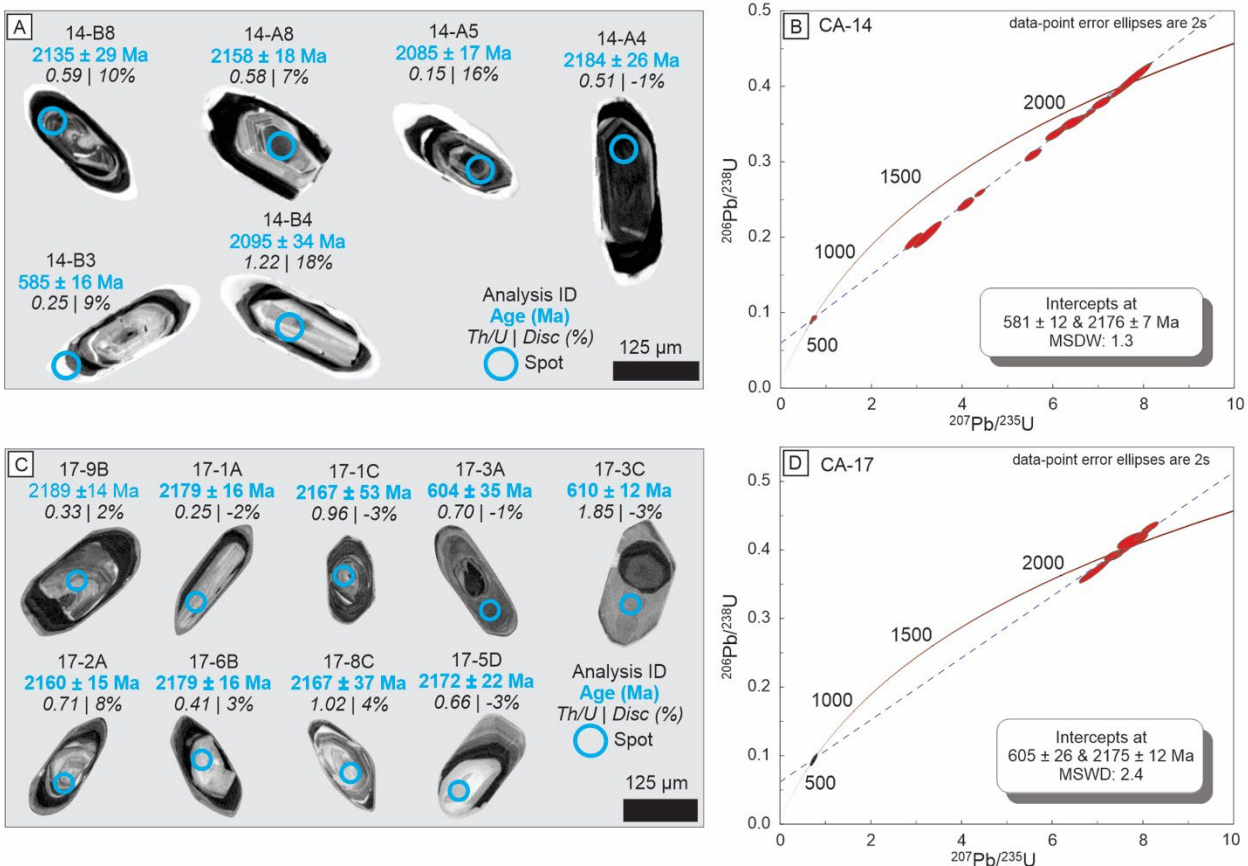
Figure 6. U-Pb concordia diagrams and cathodoluminescence images of representative zircon grains from the Juiz de Fora Complex granodioritic granulites: (A and B) sample CA-14; (C and D) sample CA-17.

Table 2. Relationships between zircon U-Pb ages and Th/U ratios obtained for the different zircon domains of the analyzed samples (CA-14 and CA-17).

Sample	Domain	Age (Ma)	Th/U	Interpretation
CA-14	Core	2176 ± 7	0.15-1.22	Crystallization age
	Rimm	581 ± 12	0.19-0.61	Metamorphism age
CA-17	Core	2175 ± 12	0.25-1.02	Crystallization age
	Rimm	605 ± 26	0.45-1.85	Metamorphism age

Table 3. Petrogenetic parameters and model age (T_{CHUR} and T_{DM}) calculated from isotopic analyzes of Sm-Nd and Sr in whole rock of the granodioritic granulites from the Juiz de Fora Complex.

Sample	CA-02	CA-14	CA-17	CA-22
Sm_{ID}	5.6	7.5	4.5	10.2
Nd_{ID}	28.0	35.5	25.7	54.2
Rb*	39.0	28.0	157.0	71.0
Sr*	624.0	542.0	414.0	377.0
$^{143}Nd/^{144}Nd_{(m)}$	0.511355	0.511573	0.511377	0.511444
Std. Err. Abs (2s)	0.000006	0.000004	0.000003	0.000006
$^{147}Sm/^{144}Nd_{(m)}$	0.1215	0.1268	0.1070	0.1132
$^{87}Sr/^{86}Sr_{(m)}$	0.716290	0.718424	0.728180	0.725007
Std. Err. Abs (2s)	0.000010	0.000011	0.000004	0.000005
Age (Ma)	2.18	2.18	2.18	2.18
$f_{Sm/Nd}$ (0 Ma)	-0.38	-0.35	-0.46	-0.42
ε_{Nd} (t)	-4.0	-1.2	0.5	0.0
ε_{Nd} (0 Ma)	-25.0	-20.8	-24.6	-23.3
T_{CHUR} (± 0.05 Ga)	2.60	2.32	2.14	2.18
T_{DM} (± 0.05 Ga)	2.59	2.31	2.13	2.17
$^{87}Sr/^{86}Sr_{(i)}$	0.7106	0.7137	0.6937	0.7079

*Values from lithogeochemical data.

magmatic arcs (Kelemen *et al.* 1993). Moderate to high Mg# is also evidence for mantle melting (Zhang *et al.* 2019, Zheng 2019) and enrichment in Ba and K suggests the participation of fluids derived from a descending plate as a metasomatic agent (Pearce and Parkinson 1993, Zheng 2019, Nielsen *et al.* 2020, Rustioni *et al.* 2021).

Based on the main geochemical characteristics highlighted above, the study rocks are interpreted to have derived from a magma sourced from the peridotitic mantle metasomatized by fluids and melts derived from subducting oceanic crust. In contrast to modern BADR magmatic arc rocks, the studied samples show characteristics which are more similar to those of the sanukite series, as described by Stern *et al.* (1989), Stern and Hanson (1991), Martin *et al.* (2005, 2010), and Heilimo *et al.* (2010): moderate to low Na_2O/K_2O ratios, and moderate to high Mg# and $(La/Yb)_N$ ratios (Table 4).

Comparing the composition of the studied rocks with that of typical sanukitoid rocks (Table 4), both are magnesian calc-alkaline with intermediate SiO_2, with high Mg#, metaluminous to weakly peraluminous, with high Ba and Sr and low Na_2O/K_2O ratios. Although Cr contents are similar to those of sanukitoids, the Ni contents of the studied samples are comparatively lower, as well as the $(La/Yb)_N$ ratios around 6.0, but significantly higher than those found in the BADRs suites (Table 3; Martin *et al.* 2005, 2010, Heilimo *et al.*

2010). Thus, given that the studied rocks present most chemical characteristics in agreement with the values expected for the sanukitic series, their chemical/tectonic classification as sanukitoid is appropriate.

Integrating the zircon U-Pb geochronology with the Sm-Nd and Sr isotopic data, the studied rocks have chondritic to slightly contaminated initial ε_{Nd} isotopic signatures, between −4.0 and 0.5. Their juvenile character is indicated by the T_{DM} model ages that are either coincident with, or slightly older than, the magmatic crystallization ages. In contrast, the initial $^{87}Sr/^{86}Sr$ ratios point to some significant crustal contribution within its metasomatized mantle source. These data imply that the mantle source of the magmas that generated these rocks features an enriched mantle signature, probably associated with the assimilation of fluids and sediments recycled back to the mantle by descending oceanic plates during protracted events of subduction in modern convergent margin settings, as discussed by Hawkesworth *et al.* (1994), Chauvel *et al.* (2008), and Zhang *et al.* (2019).

Neoproterozoic metamorphic overprint

The metamorphic ages obtained between 581 and 605 Ma are compatible with data presented in previous regional studies (Machado *et al.* 1996, Heilbron and Machado 2003, Heilbron *et al.* 2010, 2020a, 2020b, Degler *et al.* 2018, Kuribara *et al.* 2019).

Table 4. Comparison of the chemical composition of the granulitic granulites studied in the present work with the typical composition of the sanukitic series, Archean sanukitoids, Paleoproterozoic Sanukitoids, and modern arc granitoids.

	Sanukitic Serie[1,2,3]	Archean Sanukitoids[4] (n = 104)	Archean Sanukitoids of Karelian Province[5] (n = 161)	Paleoproterozoic sanukitoids of the Aravalli craton, India[6] (n = 20)	Modern arc granitoids[4] (n = 250)	Sanukitoids from northern Juiz de Fora Complex (This work)							
						Average (n = 7)	CA-11	CA-14	CA-02	CA-22	CA-23	CA-04	CA-17
SiO_2	55-73	58.65	55-70	62.01	68.1	62.52	58.41	59.78	60.62	63.50	64.56	64.99	65.79
MgO	5.2-9.17	3.90	1.5-9	1.44	1.55	2.77	2.89	3.48	3.45	2.60	2.98	2.05	1.91
K_2O	0.5-4	3.11	1.5-5	5.40	3.4	2.83	3.42	1.69	2.24	2.42	1.72	4.12	4.18
Ba	> 1,000	1,471	706-1613	1,174	715	954.43	1368	509	1197	648	489	1389	1081
Sr	> 500	1,108	513-941	213	316	477.57	455	542	624	377	449	482	414
Cr	≤ 150	104	6-184	16.7	23	67.14	40.0	110.0	90.0	70.0	50.0	50.0	60.0
Ni	90-205	54	8-85	12.6	10.5	35	< 20	50.0	< 20	< 20	< 20	< 20	20.0
Mg#	0.43-0.62	0.53	45-65	0.33	0.41	0.47	43.69	46.07	46.78	43.81	54.02	46.26	46.00
Na_2O/K_2O	~3	1.38	0.5-3	0.39	1.08	1.18	0.99	2.34	1.53	1.31	1.90	0.71	0.76
Ba+Sr	> 1,500	> 1,466*	> 1,400	1387	1,031	1432	1,823	1,051	1,821	1,025	938	1,871	1,495
$(La/Yb)_N$	-	30.5	14-47	14.95	6.4	12.66	13.7	13.44	9.55	12.18	13.72	15.15	10.85
Rb/Sr	0.01-0.16	0.08	0.10-0.13	0.69	0.35	0.17	0.18	0.05	0.06	0.17	0.16	0.24	0.38

[1]Shirey and Hanson (1984); [2]Stern *et al.* (1989); [3]Stern e Hanson (1991); [4]Martin *et al.* (2010); [5]Heilimo *et al.* (2010); [6]Raza *et al.* (2021).

During the Brasiliano/Pan-African overprint at ~580 Ma, intense deformation and regional metamorphism resulted from the collision stage of the Araçuaí-Ribeira Orogenic System (with the collision between the São Francisco Paleocontinent margin and the Inner Arc System — Rio Doce and Serra da Bolívia magmatic arcs; Heilbron and Machado 2003, Heilbron *et al.* 2017, 2020a, 2020b). As evidenced by the morphology of the zircon grains and high Th/U ratios, the high metamorphic grade of the rocks is also evidenced by mineral peak metamorphic associations typical of the granulite facies (with orthopyroxene + clinopyroxene + plagioclase) in all study samples.

The Neoproterozoic granulite metamorphism is common in the entire JFC (Duarte *et al.* 1997, 2000, Heilbron *et al.* 1998, 2010, Medeiros Júnior *et al.* 2017) and is also observed in nearby units, such as the paragneisses from the Raposos and Bom Jesus do Itabapoana groups and in the orthogneisses from the Neoproterozoic Serra da Bolivia/Rio Doce magmatic arc (Karniol *et al.* 2009, Santos *et al.* 2011, Gouvêa *et al.* 2020, Marques *et al.* 2021). In addition, the observation of hornblende and biotite partially substituting orthopyroxene and clinopyroxene in some samples suggests retrometamorphism in conditions of upper amphibolite facies, also in agreement with regional works (Santos *et al.* 2011, Ferreira *et al.* 2020, Marques *et al.* 2021).

Sanukitoid suites in the southern São Francisco Paleocontinent

Several Neoarchean to the late Rhyacian sanukitoid suites related to the accretionary processes that formed the São Francisco Paleocontinent have been previously described in the Minas Segment of the MBOS (Seixas *et al.* 2013, Moreira *et al.* 2018, Bruno *et al.* 2020, 2021a, 2021b, Araújo *et al.* 2019, 2021, Almeida *et al.* 2022). The generation of these different sanukitoid suites, mostly following the formation of TTG suites, has been interpreted as evidence of the diachronism on Earth's geodynamic processes that changes from typical Archean tectonic regimes to tectonic regimes more likely to those currently active (Moreira *et al.* 2018, 2020, Bruno *et al.* 2020, 2021a, 2021b). In order to generate more regional interpretations, the dataset obtained was compared with compiled data from different Paleoproterozoic sanukitoid suites from the Minas Segment of the MBOS (Fig. 7 and Table 5), which occur in the southern JFC (Araújo *et al.* 2019, 2021, Almeida *et al.* 2022), in the Mantiqueira Complex (Bruno *et al.* 2020) and in the Mineiro Belt (Seixas *et al.* 2013, Moreira *et al.* 2018, Bruno *et al.* 2021b). The considerations in this topic assume that the sanukitoid suites of each of these compartments have an independent (not cogenetic) evolution.

Regarding the major element compositions, all suites in question are very similar, with a predominance of rocks with intermediate SiO_2 contents and normatively classified as diorites and granodiorites (Fig. 8A). Their calc-alkaline character with high-K mafic rocks sources (Fig. 8B) is expected since they are all classified as sanukitoid rocks (Fig. 8C). When analyzing their REEs patterns (Figs. 9A and 9B), differences begin to become more noticeable. The JFC sanukitoid rocks are quite similar to the other sanukitoid rocks of the southern São Francisco Paleocontinent and, in general, all suites have similar characteristics (fractionation between LREE and HREE; absent, slightly positive, or slightly negative Eu anomalies; enrichment in LILE and depletion in HFSE). However, for the JFC sanukitoid rocks, those described in this work and in Araújo *et al.* (2021) are noticeably more enriched in LREE than those described by Almeida *et al.* (2022), where the fractionation between LREE and HREE is less expressive. This implies that these rocks were generated by lower degrees of partial melting or fractionation processes than the others. Moreover, the sanukitoid rocks of the southern JFC described by Almeida *et al.* (2022) show higher enrichment in fluid-mobile elements (*e.g.*, Ba and Sr; Zheng 2019, Nielsen *et al.* 2020) and depletion in Th (melt-mobile; Zheng 2019).
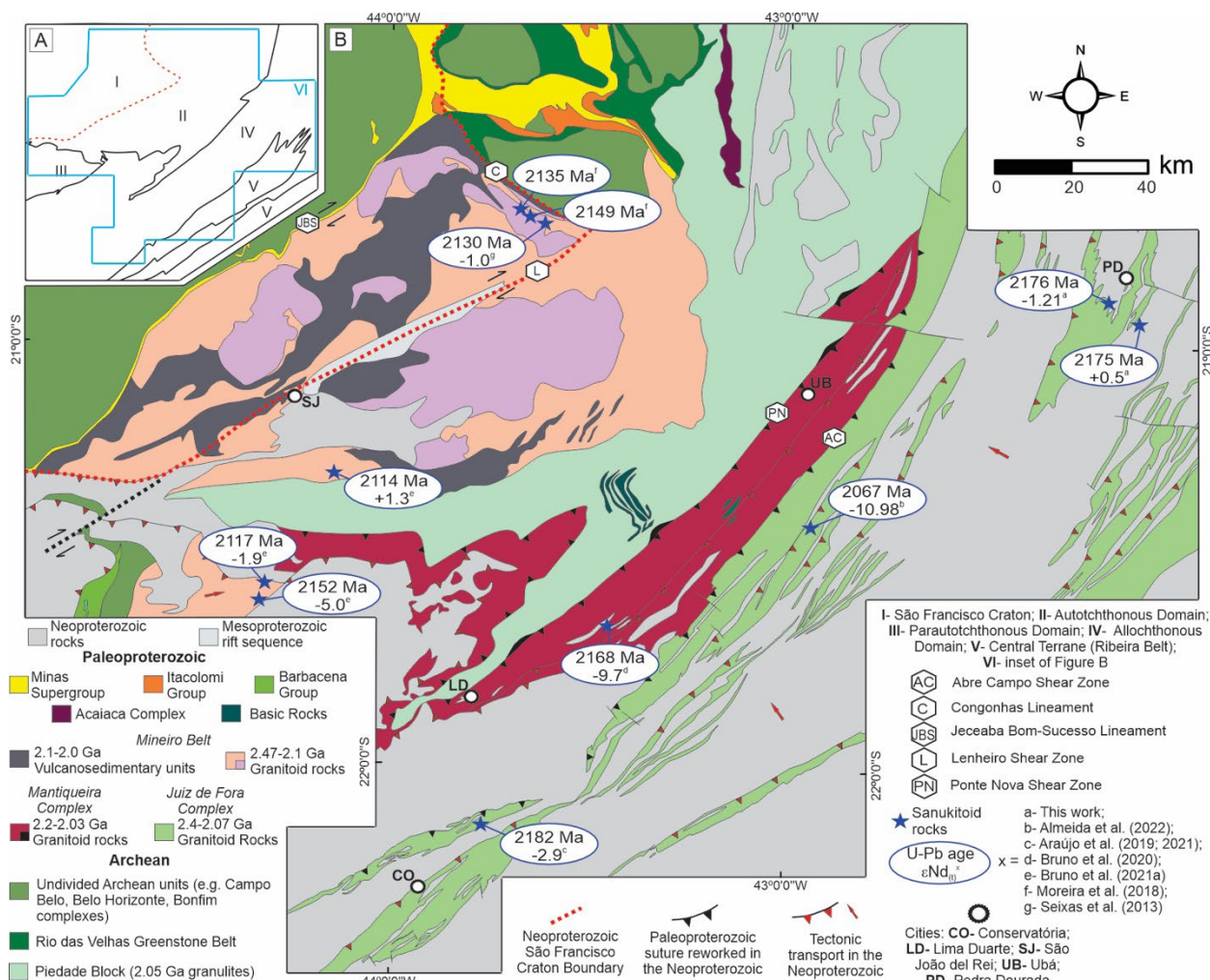
Source: Seixas *et al.* (2013), Moreira *et al.* (2018), Araújo *et al.* (2019, 2021), Bruno *et al.* (2020, 2021b), and Almeida *et al.* (2022).

Figure 7. Location of sanukitoid occurrences in southern São Francisco Paleocontinent. (A) Regional tectonic-structural compartmentalization and (B) simplified regional geological map and sanukitoid rocks occurrences (with U-Pb and Sm-Nd data).

Table 5. Comparison of the different Paleoproterozoic sanukitoid suites from the south of the São Francisco Paleocontinent with ages of magmatic crystallization, initial ε_{Nd}, and T_{DM}.

Unit	Lithotypes	Age (Ma)	$\varepsilon Nd_{(t)}$	T_{DM} (Ga) (± 0.05)	References
Juiz de Fora Complex	Granodioritic granulites	2176 to 2175	-4.0 to + 0.5	2.57 to 2.12	This work
	Charno-enderbitic granulite	2200 to 2180	-4.8 to -2.9	2.62 to 2.46	Araújo *et al.* (2019, 2021)
	Enderbitic orthogranulite	2068	-11.0	3.05	Almeida *et al.* (2022)
Mantiqueira Complex	Hbl-Bt orthogneiss	2168	-9.7	3.18	Bruno *et al.* (2020)
Mineiro Belt	Tonalite	2130	-0.8 to + 0.9	2.40 to 2.30	Seixas *et al.* (2013)
	Bt-Hbl tonalites	2149 to 2135	-	-	Moreira *et al.* (2018)
	Granodioritic Hbl-Bt orthogneiss	2152 to 2114	-5.0 to + 1.3	2.64 to 2.21	Bruno et al. (2021b)

The differences between these different sanukitoid suites become more explicit when their crystallization ages and their Sm-Nd isotopic signatures are compared (Table 5, and Figs. 7 and 10). In general, most of them (the sanukitoid suites of the JFC, Mantiqueira Complex, and Mineiro Belt) have Rhyacian crystallization ages, initial ε_{Nd} between −5.0 and +1.3 (moderately juvenile), and Neoarchean to Siderian and Rhyacian T_{DM} Nd model ages. The exceptions are the sanukitoid rocks of the southern CJF (Almeida *et al.* 2022) and Mantiqueira Complex (Bruno *et al.* 2020), both with significantly lower initial ε_{Nd} (−10.98 and −9.7, respectively) and Mesoarchean T_{DM} ages.

In addition, the southern JFC sanukitoid rocks described by Almeida *et al.* (2022), with a crystallization age of 2068 Ma, are the youngest sanukitoid rocks reported from the southern São Francisco Paleocontinent.

In the regional scenario (Fig. 7), the integration and analysis of these data suggest that the rocks from the Minas segment of the MBOS, in the southern São Francisco Paleocontinent, record at least two stages of sanukitoid generation: the first and more long-lived event, between 2.20 and 2.11 Ga, is coincident with the climax of juvenile crust formation within the Minas Segment of the MBOS and coeval with the generation of different
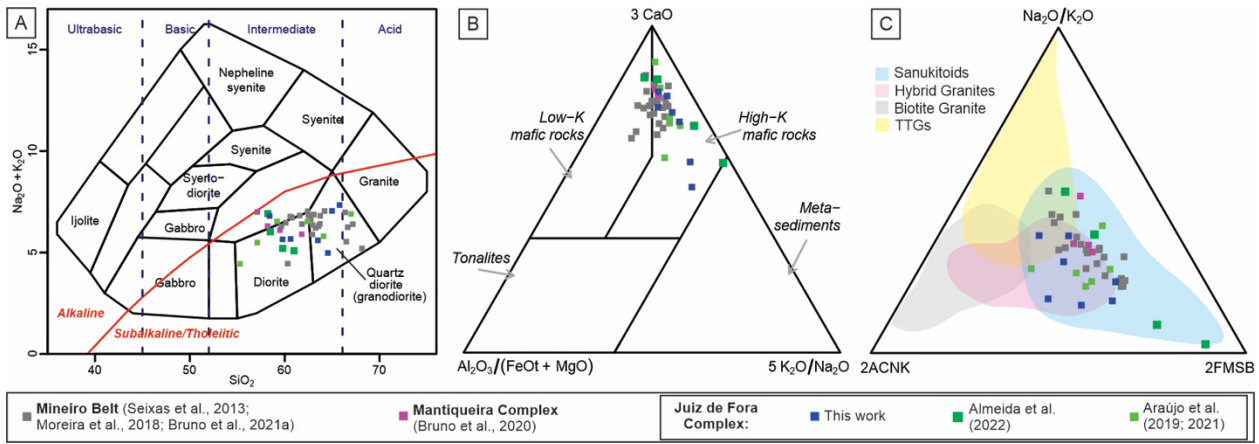
Figure 8. Comparison of major element composition of sanukitoid suites from southern São Francisco Paleocontinent: (A) TAS diagram of Cox *et al.* (1979); (B) source diagram of Laurent *et al.* (2014); (C) ternary classification diagram for late-Archean granitoids of Laurent *et al.* (2014).
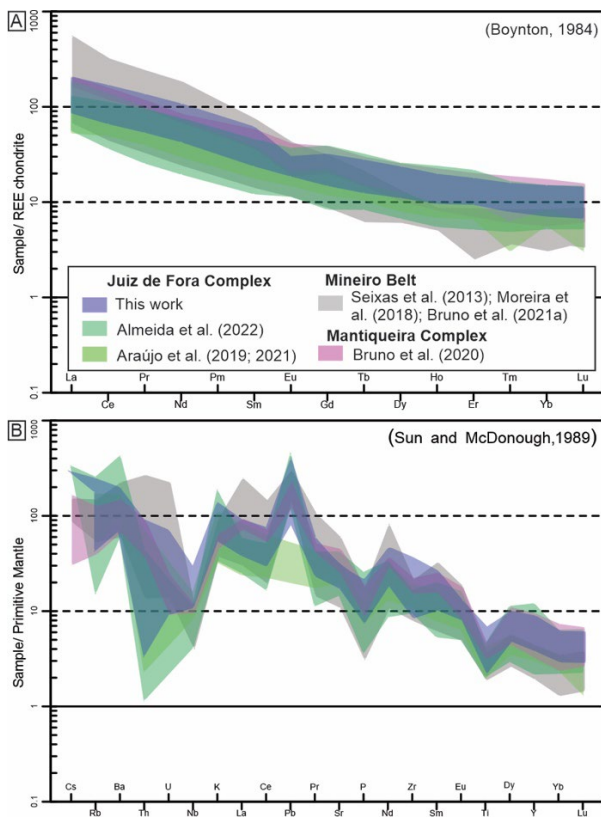

Figure 9. REE patterns of the different sanukitoid suites from southern São Francisco Paleocontinent: (A) chondrite-normalized REE (Boynton 1984) and (B) primitive mantle-normalized REE (Sun and McDonough 1989).
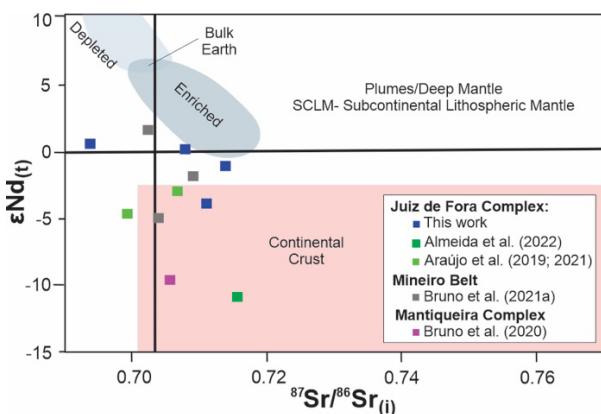
Figure 10. Initial ε_{Nd} versus initial $^{87}Sr/^{86}Sr$ of the different sanukitoid suites from the southern São Francisco Paleocontinent.

sanukitoid suites (along with TTG suites and granitoid rocks) from the Mineiro Belt (Seixas *et al.* 2013, Moreira *et al.* 2018, Bruno *et al.* 2021b) and the Mantiqueira and JFC complexes (Bruno *et al.* 2020, Araújo *et al.* 2021; and this work); the second and younger event, dated at ca. 2.07 Ga, is restricted to the JFC (Almeida *et al.* 2022) and was emplaced immediately before the regional metamorphism resulting from the diachronic collision of Archean blocks and Paleoproterozoic magmatic arcs during the final stages of São Francisco Paleocontinent amalgamation, as suggested by the emplacement of syn-collisional granitoid rocks and metamorphism ages between 2.05 Ga in Mineiro Belt (Moreira *et al.* 2018, Bruno *et al.* 2020, 2021b) and 2.03 Ga in the JFC (Araújo *et al.* 2021).

Regarding the geodynamic processes responsible for the generation of these rocks, the generation of pre-collisional rocks with a sanukitoid signature in the midst of calc-alkaline granitoid suites, magmatic arc tholeiites, and TTG suites allows the interpretation of a scenario with a complex accretionary system during the Paleoproterozoic in these different compartments (i.e., Mineiro, and the Mantiqueira and Juiz de Fora complexes; Fig. 11). In contrast to the typical sanukites, the sanukitoid magmatic arc signature depicted by the rocks from the Minas Orogen shows a lower fractionation between LREE and HREE, with intermediate $(La/Yb)_N$ ratios between typical Archean sanukitoid and BADR suites from modern magmatic arcs. This difference implies lower degrees of interaction between melts from the subducting plate and the peridotite mantle, limiting the metasomatism of the mantle wedge in the subduction zone almost exclusively by fluids released from the descending plate at depth, in a process that is intermediate between the generation of typical sanukitoids and modern BADR suites, which is possible with an increase in the dip angle of the descending plate, as presented by Martin *et al.* (2010). Regarding the sources of these rocks, the initial ε_{Nd} varying between close to 0 and −11 (Table 5 and Fig. 10) attest to the origin of these magmas in a hybrid mantle, significantly modified by the assimilation of crustal material (fluids and melt) from the subducting plate and sediments carried out into the mantle by the descending slab over an extended period of time and/or by earlier subduction processes, as discussed by Hawkesworth *et al.* (1994), Chauvel *et al.* (2008), and Zhang *et al.* (2019).
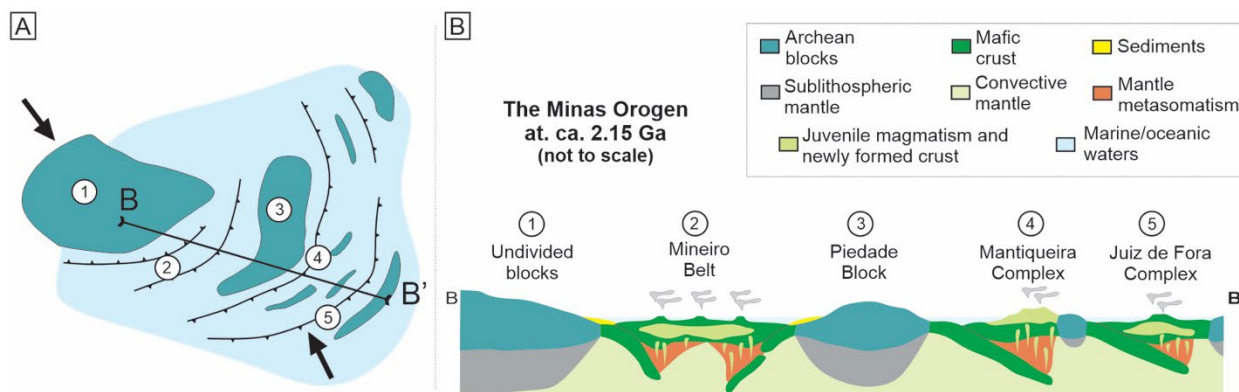
Figure 11. The Minas Orogen at about 2.15 Ga: (A) paleogeographic reconstruction of the configuration of the crustal blocks and magmatic arcs of southeastern São Francisco Paleocontinent at ca. from 2.15 Ga (modified from Alkmim and Teixeira 2017, Bruno *et al.* 2021b) and (B) schematic tectonic cross-section of the generation of mantle-derived rocks (*e.g.*, sanukitoids) in the Mineiro Belt and in the Mantiqueira and Juiz de Fora complexes in ca. of 2.15 Ga (modified from Bruno *et al.* 2021a).

CONCLUSIONS

The study rocks are granodioritic granulites, with chemical characteristics compatible with those of sanukitoid rocks: they are intermediate SiO_2, with moderate to high Ba, Sr, Mg#, high $(La/Yb)_N$ ratio, and low Na_2O/K_2O ratio. They are crystallized at ca. 2175 Ma and underwent high-grade metamorphism at ca. 605–580 Ma during the Brasiliano orogenic events. In addition, initial εNd between −4.0 and +0.5, T_{DM} between 2.57 and 2.12 Ga, and initial $^{87}Sr/^{86}Sr$ ratios between 0.6937 to 0.7137 are typical of moderately juvenile to slightly evolved (contaminated?) isotope sources and suggest that the genesis of these rocks is related to a hybrid mantle source contaminated with crustal material (fluids, sediments, and melts) during protracted periods of subduction and/or by previous subductions.

In the Paleoproterozoic scenario of the southern São Francisco Paleocontinent, there are at least two periods of generation of magmatic arc rocks with sanukitoid signatures, namely, the first one, between 2.20 and 2.11 Ga, is associated with calc-alkaline granitoid rocks, IAT and TTG rocks in the Mineiro Belt, Mantiqueira, and JFC complexes; and a younger one, restricted to the JFC, with the generation of sanukitoid rocks and calc-alkaline granitoid and TTG rocks at ca. 2.07 Ga. Such rock associations with distinct signatures attest to a complex and enduring accretionary system to the southeast of the São Francisco Paleocontinent during the Rhyacian (within the Minas Segment), very similar to those of modern plate tectonics accretionary settings.

REFERENCES

Alkmim F.F., Teixeira W. 2017. The Paleoproterozoic Mineiro Belt and the Quadrilátero Ferrífero. In: Heilbron M., Cordani U., Alkmim F.F. (eds.). *São Francisco Craton, Eastern Brazil: Tectonic Genealogy of a Miniature Continent*. Springer, v. 1, p. 71-94. https://doi.org/10.1007/978-3-319-01715-0_5

Almeida R., Elizeu V., Bruno H., Bersan S.M., Araújo L.E.A.B., Dussin I., Valeriano C.M., Neto C., Heilbron M. 2021. Rhyacian-Orosirian tectonic history of the Juiz de Fora Complex: evidence for an Archean crustal reservoir within an island-arc system. *Geosciences Frontiers*, **13**(5):101292. https://doi.org/10.1016/j.gsf.2021.101292

André J.L.F., Valladares C.S., Duarte B.P. 2009. O Complexo Juiz de Fora na região de Três Rios (RJ): litogeoquímica, geocronologia U-Pb (LA-ICPMS) e geoquímica isotópica de Nd e Sr. *Revista Brasileira de Geociências*, **39**(4):773-793.

Araújo L.E.A.B., Heilbron M., Teixeira W., Dussin I.A., Valeriano C.M., Bruno H., Sato K., Paravidini G., Castro M. 2021. Siderian to Rhyacian evolution of the Juiz de Fora Complex: arc fingerprints and correlations within the Minas-Bahia Orogen and the Western Central Africa Belt. *Precambrian Research*, **359**:106118. https://doi.org/10.1016/j.precamres.2021.106118

Araújo L.E.A.B., Heilbron M., Valeriano C.M., Teixeira W., Aguiar Neto C.C. 2019. Lithogeochemical and Nd-Sr isotope data of the orthogranulites of the Juiz de Fora Complex, SE-Brazil: insights from a hidden Rhyacian Orogen within the Ribeira belt. *Brazilian Journal of Geology*, **49**(3):e20190007. https://doi.org/10.1590/2317-4889201920190007

Ávila C.A., Teixeira W., Bongiolo E.M., Dussin I.A., Vieira T.A.T. 2014. Rhyacian evolution of subvolcanic and metasedimentary rocks of the southern segment of the Mineiro belt, São Francisco Craton, Brazil. *Precambrian Research*, **243**:221-251. https://doi.org/10.1016/j.precamres.2013.12.028

Ávila C.A., Teixeira W., Cordani U.G., Moura C.A.V., Pereira R.M. 2010. Rhyacian (2.23–2.20 Ga) juvenile accretion in the southern São Francisco craton, Brazil: geochemical and isotopic evidence from the Serrinha magmatic suite, Mineiro belt. *Journal of South American Earth Sciences*, **29**(2):464-482. https://doi.org/10.1016/j.jsames.2009.07.009

Barbosa J.S.F., Barbosa R.G. 2017. The Paleoproterozoic Eastern Bahia orogenic domain. In: Heilbron M., Cordani U.G., Alkmim F. (eds.). *The São Francisco Craton, Eastern Brazil: Tectônic Genealogy of a Miniature Continent*. Springer, v. 1, p. 57-70. https://doi.org/10.1007/978-3-319-01715-0_4

Barbosa N.S., Teixeira W., Ávila C.A., Montecinos P.M., Bongiolo E.M. 2015. 2.17–2.10 Ga plutonic episodes in the Mineiro belt, São Francisco Craton, Brazil: U-Pb ages, geochemical constraints and tectonics. *Precambrian Research*, **270**:204-225. https://doi.org/10.1016/j.precamres.2015.09.010

Bersan S.M., Costa A.F.O., Danderfer A., Abreu F.R., Lana C., Queiroga G., Storey C., Moreira H. 2020. Paleoproterozoic juvenile magmatism within the northeastern sector of the São Francisco paleocontinent: insights from the shoshonitic high Ba–Sr Montezuma granitoids. *Geosciences Frontiers*, **11**(5):1821-1840. https://doi.org/10.1016/j.gsf.2020.01.017

Boynton W.V. 1984. Cosmochemistry of the rare earth elements; meteorite studies. In: Henderson P. (ed.). *Rare Earth Element* Geochemistry. Amsterdam: Elsevier, p. 63-114. https://doi.org/10.1016/B978-0-444-42148-7.50008-3

Bruno H., Elizeu V., Heilbron M., Valeriano C.M., Strachan R., Fowler M., Bersan S., Moreira H., Dussin I., Silva L.G.E., Tupinambá M., Almeida J.C.H., Neto C., Storey C. 2020. Neoarchean and Rhyacian TTG-Sanukitoid suites in the Southern São Francisco Paleocontinent, Brazil: evidence for diachronous change towards modern tectonics. *Geosciences Frontiers*, **11**(5):1763-1787. https://doi.org/10.1016/j.gsf.2020.01.015

Bruno H., Heilbron M., Strachan R., Fowler M., Valeriano C.M., Bersan S., Moreira H., Cutts K., Dunlop J., Almeida R., Almeida J., Storey C. 2021a. Earth's new tectonic regime at the dawn of the Paleoproterozoic: Hf isotope evidence for efficient crustal growth and reworking in the São Francisco craton, Brazil. *Geology*, **49**(10):1214-1219. https://doi.org/10.1130/G49024.1

Bruno H., Heilbron M., Valeriano C.M., Strachan R., Fowler M., Bersan S., Moreira H., Motta R., Almeida J., Almeida R., Carvalho M., Storey C. 2021b. Evidence for a complex accretionary history preceding the amalgamation of Columbia: the Rhyacian Minas-Bahia Orogen, southern São Francisco Paleocontinent, Brazil. *Gondwana Research*, **92**:149-171. https://doi.org/10.1016/j.gr.2020.12.019

Cawood P.A., Kröner A., Collins W.J., Kusky T.M., Mooney W.D., Windley B.F. 2009. Accretionary orogens through Earth history. In: Cawood P.A., Kröner A. (eds). *Earth accretionary systems in space and time*. London: The Geological Society, v. 318, p. 1-36. https://doi.org/10.1144/SP318.1

Caxito F.A., Hartmann L.A., Heilbron M., Pedrosa-Soares A.C., Bruno H., Basei M.A.S., Chemale F. 2022. Multi-proxy evidence for subduction of the Neoproterozoic Adamastor Ocean and Wilson cycle tectonics in the South Atlantic Brasiliano Orogenic System of Western Gondwana. *Precambrian Research*, **376**(15):106678. https://doi.org/10.1016/j.precamres.2022.106678

Chauvel C., Lewin E., Carpentier M., Arndt N., Marini F-C. 2008. Role of recycled oceanic basalt and sediment in generating the Hf–Nd mantle array. *Nature Geoscience*, **1**:64-67. https://doi.org/10.1038/ngeo.2007.51

Condie K.C. 2005. TTGs and adakites: are they both slab melts? *Lithos*, **80**(1-4):33-44. https://doi.org/10.1016/j.lithos.2003.11.001

Cox K.G., Bell J.D., Pankhurst R.J. 1979. *The Interpretation of Igneous Rocks*. London: Allen & Unwin.

Cutts K., Lana C., Moreira H., Alkmim F., Peres G.G. 2020. Zircon U-Pb and Lu-Hf record from high-grade complexes within the Mantiqueira Complex: first evidence of juvenile crustal input at 2.4–2.2 Ga and implications for the Paleoproterozoic evolution of the São Francisco Craton. *Precambrian Research*, **338**:105567. https://doi.org/10.1016/j.precamres.2019.105567

Degler R., Pedrosa-Soares A., Novo T., Tedeschi M., Silva L.C., Dussin I., Lana C. 2018. Rhyacian-Orosirian isotopic records from the basement of the Araçuaí-Ribeira orogenic system (SE Brazil): links in the Congo-São Francisco paleocontinent. *Precambrian Research*, **317**:179-195. https://doi.org/10.1016/j.precamres.2018.08.018

Duarte B.P., Figueiredo M.C.H., Campos Neto M., Heilbron M. 1997. Geochemistry of the granulite facies orthogneisses of Juiz de Fora Complex, Central Segment of the Ribeira Belt, Southeastern Brazil. *Revista Brasileira de Geociências*, **27**(1):67-82. http://doi.org/10.25249/0375-7536.19976782

Duarte B.P., Heilbron M., Campos Neto M.C. 2000. Granulite/charnockite from the Juiz de Fora Domain, Central Segment of the Brasiliano-Pan-African Ribeira Belt. *Revista Brasileira de Geociências*, **30**(3):358-362.

Duarte B.P., Valente S.C., Heilbron M., Campos Neto M.C. 2004. Petrogenesis of the Orthogneisses of the Mantiqueira Complex, Central Ribeira Belt, SE Brazil: An Archaean to Palaeoproterozoic Basement Unit Reworked During the Pan-African Orogeny. *Gondwana Research*, **7**(2):437-450. https://doi.org/10.1016/S1342-937X(05)70795-4

Faria T.G., Alves M.I., Potratz G.L., Silva L.F., Rodrigues S.W.O., Martins M.V.A., Geraldes M.C. 2022. The Serra do Caparaó Complex, Mantiqueira Province, Brazil, revisited: metamorphic age constraints by U-Pb and Lu-Hf method in zircon by LA-ICP-MS. *Journal of the Geological Survey of Brazil*, **5**(1):49-80. https://doi.org/10.29396/jgsb.2022.v5.n1.1

Ferreira S.L.M., Marques R.A., Melo M.G., Medeiros Junior E.B., Reis S.V., Silva R.M., Valle H.F., Queiroga G.N. 2020. Petrografia e termobarometria de granitoides diatexíticos portadores de anfibólio da região de São José de Ubá e São João do Paraíso. *Geologia USP*. Série Científica, **20**(4):23-37. https://doi.org/10.11606/issn.2316-9095.v20-167607

Foley S.F., Tiepolo M., Vannucci R. 2002. Growth of early continental crust controlled by melting of amphibolite in subduction zones. *Nature*, **417**:837-840. https://doi.org/10.1038/nature00799

Fowler M., Rollinson H. 2012. Phanerozoic sanukitoids from Caledonian Scotland: Implications for Archean subduction. *Geology*, **40**(12):1079-1082. https://doi.org/10.1130/G33371.1

Frost B.R., Barnes C.G., Collins W.J., Arculus R.J., Ellis D.J., Frost C.D. 2001. A geochemical classification for granitic rocks. *Journal of Petrology*, **42**(11):2033-2048. https://doi.org/10.1093/petrology/42.11.2033

Gouvêa L.P., Medeiros S.R., Mendes J.C., Soares C.C., Marques R., Melo M. 2020. Magmatic activity period and estimation of P-T metamorphic conditions of pre-collisional opx-metatonalite from Araçuaí-Ribeira orogens boundary, SE Brazil. *Journal of South American Earth Sciences*, **99**:102506. https://doi.org/10.1016/j.jsames.2020.102506

Grochowski J., Kuchenbecker M., Barbuena D., Novo T. 2021. Disclosing Rhyacian/Orosirian orogenic magmatism within the Guanhães basement inlier, Araçuaí Orogen, Brazil: a new piece on the assembly of the São Francisco-Congo paleocontinent. *Precambrian Research*, **363**:106329. https://doi.org/10.1016/j.precamres.2021.106329

Hawkesworth C.J., Dhuime B., Pietranik A.B., Cawood P.A., Kemp A.I.S., Storey C.D. 2010. The generation and evolution of the continental crust. *Journal of Geological Society*, **167**(2):229-248. https://doi.org/10.1144/0016-76492009-072

Hawkesworth C.J., Gallagher K., Hergt J.M., McDermott F. 1994. Destructive plate margin magmatism: geochemistry and melt generation. *Lithos*, **33**(1-3):169-188. https://doi.org/10.1016/0024-4937(94)90059-0

Heilbron M., Duarte B.P., Nogueira J.R. 1998. The Juiz de Fora Granulite Complex of the Central Ribeira Belt, SE Brazil: A Paleoproterozoic Crustal Segment Thrust During the Pan-African Orogeny. *Gondwana Research*, **1**(3-4):373-381. https://doi.org/10.1016/S1342-937X(05)70853-4

Heilbron M., Duarte B.P., Valeriano C.M., Simonetti A., Machado N., Nogueira J.R. 2010. Evolution of reworked Paleoproterozoic basement

rocks within the Ribeira belt (Neoproterozoic), SE-Brazil, based on U-Pb geochronology: implications for paleogeographic reconstructions of the São Francisco-Congo paleocontinent. *Precambrian Research*, **178**(1-4):136-148. https://doi.org/10.1016/j.precamres.2010.02.002

Heilbron M., Euzébio R., Peixoto C., Tupinambá M., Guia C., Peternel R., Silva L.G., Ragatky C.D. 2013. O Complexo Juiz de Fora na Folha Santo Antônio de Pádua 1:100.000: geologia e geoquímica. *Geociências*, **32**(1):10-23.

Heilbron M., Machado N. 2003. Timing of terrane accretion in the Neoproterozoic-Eopaleozoic Ribeira Orogen (SE Brazil). *Precambrian Research*, **125**(1-2):87-112. https://doi.org/10.1016/S0301-9268(03)00082-2

Heilbron M., Ribeiro A., Valeriano C.M., Paciullo F.V.P., Almeida J.C.H., Trouw R.A.J., Tupinamba M., Silva L.G.E. 2017. The Ribeira belt. In: Heilbron M., Cordani U.G., Alkmim F.F. (eds.), *São Francisco Craton, Eastern Brazil: Tectonic Genealogy of a Miniature Continent*. Switzerland, Springer, p. 277-304. https://doi.org/10.1007/978-3-319-01715-0

Heilbron H., Silva L.G.E., Almeida J.C.H., Tupinambá M., Peixoto C., Valeriano C.M., Lobato M., Rodrigues S.W.O., Ragatky C.D., Silva M.A., Monteiro T., ªreitas N., Miguens D., Girão R. 2020a. Proterozoic to Ordovician geology and tectonic evolution of Rio de Janeiro State, SE-Brazil: insights on the central Ribeira Orogen from the new 1:400,000 scale geologic map. *Brazilian Journal of Geology*, **50**(2):e20190099. https://doi.org/10.1590/2317-4889202020190099

Heilbron M., Valeriano C.M., Peixoto C., Tupinambá M., Neubauer F., Dussin I., Corrales F., Bruno H., Lobato M., Almeida, J.C.H., Eirado Silva, L.G. 2020b. Neoproterozoic magmatic arc systems of the central Ribeira belt, SE-Brazil, in the context of the West-Gondwana pre-collisional history: a review. *Journal of South American Earth Sciences*, **103**:102710. https://doi.org/10.1016/j.jsames.2020.102710

Heilimo E., Halla J., Höttä P. 2010. Discrimination and origin of the sanukitoid series: geochemical constraints from the Neoarchean western Karelian Province (Finland). *Lithos*, **115**(1-4):27-39. https://doi.org/10.1016/j.lithos.2009.11.001

Karniol T.R., Machado R., Bilal E., Moutte J. 2009. Geotermobarometria de granulitos do Cinturão Ribeira na porção norte do estado do Rio de Janeiro: seção Italva (RJ) – Patrocínio do Muriaé (MG). *Revista Brasileira de Geociências*, **39**(3):519-532.

Kelemen P.B., Shimizu N., Dunn T. 1993. Relative depletion of niobium in some arc magmas and the continental crust: partitioning of K, Nb, La and Ce during melt/rock reaction in the upper mantle. *Earth and Planetary Science Letters*, **120**(3-4):111-134. https://doi.org/10.1016/0012-821X(93)90234-Z

Kuribara Y., Tsunogae T., Santosh M., Takamura Y., Costa A., Rosière C. 2019. Eoarchean to Neoproterozoic crustal evolutioI the Mantiqueira and the Juiz de Fora Complexes, SE Brazil: petrology, geochemistry, zircon U-Pb geochronology and Lu-Hf isotopes. *Precambrian Research*, **323**:82-101. https://doi.org/10.1016/j.precamres.2019.01.008

Laurent O., Doucelance R., Martin H., Moyen J-F. 2013. Differentiation of the late-Archaean sanukitoid series and some implications for crustal growth: insights from geochemical modelling on the Bulai pluton, Central Limpopo Belt, South Africa. *Precambrian Research*, **227**:186-203. https://doi.org/10.1016/j.precamres.2012.07.004

Laurent O., Martin H., Moyen J.F., Doucelance R. 2014. The diversity and evolution of late Archean granitoids: evidence for the onset of 'modern-style' plate tectonics between 3.0 and 2.5 Ga. *Lithos*, **205**:208-235. https://doi.org/10.1016/j.lithos.2014.06.012

Machado N., Valladares C.S., Heilbron M., Valeriano C.M. 1996. U-Pb geochronology of the central Ribeira Belt (Brazil) and implications for the evolution of the Brazilian Orogeny. *Precambrian Research*, **79**(3-4):347-361. https://doi.org/10.1016/0301-9268(95)00103-4

Marques R.A., Duarte B.P., Tupinambá M.A., Medeiros Junior E.B., Mauri S. 2021. Contrasting P-T conditions of Oriental Terrane and Central Superterrane (Ribeira Belt), NW of Rio de Janeiro state, Brazil. *Pesquisas em Geociências*, **48**(3):e108406. https://doi.org/10.22456/1807-9806.108406

Martin H., Moyen J-F., Rapp R. 2010. The sanukitoid series: magmatism at the Archaean-Proterozoic transition. Earth and Environmental Science *Transactions of the Royal Society of Edinburgh*, **100**(1-2):15-33. https://doi.org/10.1017/S1755691009016120

Martin H., Smithies R.H., Rapp R., Moyen J.-F., Champion D. 2005. An overview of adakite, tonalite-trondhjemite-granodiorite (TTG), and sanukitoid: relationships and some implications for crustal evolution. *Lithos*, **79**(1-2):1-24. https://doi.org/10.1016/j.lithos.2004.04.048

Medeiros Júnior E.B., Jordt-Evangelista H., Marques R.A., Velasco T.C., Soares C.C.V. 2017. Geothermobarometry of granulites of the Juiz de Fora Complex and the Andrelândia Group in the region of Abre Campo and Manhuaçu, Minas Gerais, Brazil. *Geociências*, **36**(3):437-446. https://doi.org/10.5016/geociencias.v36i3.10943

Moreira H., Seixas L., Storey C., Fowler M., Lasalle S., Stevenson R., Lana C. 2018. Evolution of Siderian juvenile crust to Rhyacian high Ba-Sr magmatism in the Mineiro Belt, southern São Francisco Craton. *Geosciences Frontiers*, **9**(4):977-995. https://doi.org/10.1016/j.gsf.2018.01.009

Moreira H., Storey C. Fowler M., Seixas L., Dunlop J. 2020. Petrogenetic processes at the tipping point of plate tectonics: Hf-O isotope ternary modelling of Earth's last TTG to sanukitoid transition. *Earth and Planetary Science Letters*, **551**:116558. https://doi.org/10.1016/j.epsl.2020.116558

Moyen J.F., Laurent O. 2018. Archean tectonic systems? a view from igneous rocks. *Lithos*, **302-303**:99-125. https://doi.org/10.1016/j.lithos.2017.11.038

Moyen J.F., Martin H. 2012. Forty years of TTG research. *Lithos*, **148**:312-336. https://doi.org/10.1016/j.lithos.2012.06.010

Nielsen S.G., Shu Y., Auro M., Yogodzinski G., Shinjo R., Plank T., Kay S.M., Horner T.J., 2020. Barium isotope systematics of subduction zones. *Geochimica et Cosmochimica Acta*, **275**:1-18. https://doi.org/10.1016/j.gca.2020.02.006

Niu Y., O'Hara M.J. 2009. MORB mantle hosts the missing Eu (Sr, Nb, Ta and Ti) in the continental crust: new perspectives on crustal growth, crust–mantle differentiation and chemical structure of oceanic upper mantle. *Lithos*, **112**(1-2):1-17. https://doi.org/10.1016/j.lithos.2008.12.009

Noce C.M., Novo T.A., Figueiredo C.M.S., Pedrosa-Soares A.C. 2009. *Folha SF.23-X-B-VI Carangola, escala 1:100.000*. Belo Horizonte: CPRM/UFMG.

Noce C.M., Pedrosa-Soares A.C., Silva L.C., Armstrong R., Piuzana D. 2007. Evolution of polycyclic basement complexes in the Araçuaí Orogen, based on U–Pb SHRIMP data: implication for Brazil-Africa links in Paleoproterozoic time. *Precambrian Research*, **159**(1-2):60-78. https://doi.org/10.1016/j.precamres.2007.06.001

Noce C.M., Teixeira W., Quéméneur J.J.G., Martins V.T.S., Bolzachini E. 2000. Isotopic signatures of Paleoproterozoic granitoids from southern São Francisco Craton, NE Brazil, and implications for the evolution of the Transamazonian Orogeny. *Journal of South American Earth Sciences*, **13**(3):225-239. https://doi.org/10.1016/S0895-9811(00)00019-5

Novo T.A. 2009. *Significado geotectônico das rochas charnockíticas da região de Carangola: implicações para a conexão Araçuaí-Ribeira*. MS Dissertation, Instituto de Geociências, Universidade Federal de Minas Gerais, Belo Horizonte, 96 p.

Novo T.A., Noce C.M., Pedrosa-Soares A.C., Batista G.A.P. 2011. Rochas granulíticas da Suíte Caparaó na região do Pico da Bandeira: embasamento oriental do Orógeno Araçuaí. *Geonomos*, **19**(2):70-77. https://doi.org/10.18285/geonomos.v19i2.42

Oliveira M.A., Dall'Agnol R., Althoff F.J., Leite A.A.S. 2009. Mesoarchean sanukitoid rocks of the Rio Maria Granite-Greenstone Terrane, Amazonian craton, Brazil. *Journal of South American Earth Sciences*, **27**(2-3):146-160. https://doi.org/10.1016/j.jsames.2008.07.003

Oliveira M.A., Dall'Agnol R., Scaillet B. 2010. Petrological constraints on crystallization conditions of Mesoarchean Sanukitoid Rocks, Southeastern Amazonian Craton, Brazil. *Journal of Petrology*, **51**(10):2121-2148. https://doi.org/10.1093/petrology/egq051

Paciullo F.V.P., Ribeiro A., Andreis R.R., Trouw R.A.J. 2000. The Andrelândia Basin, a Neoproterozoic intraplate continental margin, Southern Brasília Belt, Brazil. *Revista Brasileira de Geociências*, **30**(1):200-202.

Pearce J.A., Parkinson I.J. 1993. Trace element models for mantle melting: application to volcanic arc petrogenesis. *Geological Society of London: Special Publications*, **76**(1):373-403. https://doi.org/10.1144/GSL.SP.1993.076.01.19

Pedrosa-Soares A.C., Noce C.M., Wiedemann C.M., Pinto C.P. 2001. The Araçuaí-West-Congo Orogen in Brazil: an overview of a confined orogen

formed during Gondwanaland assembly. *Precambrian Research*, **110**(1-4):307-323. https://doi.org/10.1016/S0301-9268(01)00174-7

Raza A., Guha D.B., Neogi S. 2021. Geochemistry of late paleoproterozoic Anjana and Amet granites of the Aravalli craton with affinities to sanukitoid series granitoids: implications for petrogenetic and geodynamic processes. *Geochemistry*, **81**(2):125758. https://doi.org/10.1016/j.chemer.2021.125758

Rustioni G., Audetat A., Keppler H. 2021. The composition of subduction zone fluids of the origin of the trace element enrichment in arc magmas. *Contributions to Mineralogy and Petrology*, **176**:51. https://doi.org/10.1007/s00410-021-01810-8

Santos B.T.M., Munhá J.M., Tassinari C.C.G., Fonseca P.E., Dias Neto C. 2011. Metamorphic P-T evolution of granulites in the central Ribeira Fold Belt, SE Brazil. *Geosciences Journal*, **15**:27-51. https://doi.org/10.1007/s12303-011-0004-1

Seixas L.A.R., Bardintzeff J.M., Stevenson R., Bonin B. 2013. Petrology of the high-Mg tonalites and dioritic enclaves of the ca. 2130 Ma Alto Maranhão suite: evidence for a major juvenile crustal addition event during the Rhyacian orogenesis, Mineiro Belt, Southeast Brazil. *Precambrian Research*, **238**:18-41. https://doi.org/10.1016/j.precamres.2013.09.015

Seixas L.A.R., David J., Stevenson R. 2012. Geochemistry, Nd isotopes and U–Pb geochronology of a 2350 Ma TTG suite, Minas Gerais, Brazil: implications for the crustal evolution of the southern São Francisco craton. *Precambrian Research*, **196-197**:61-80. https://doi.org/10.1016/j.precamres.2011.11.002

Semprich J., Moreno J.A., Oliveira E.P. 2015. Phase equilibria and trace element modeling of Archean sanukitoid melts. *Precambrian Research*, **269**:122-138. https://doi.org/10.1016/j.precamres.2015.08.004

Shand S.J. 1943. *Eruptive Rocks*. 2. ed. New York: John Wiley. 444 p.

Shirey S.B., Hanson G.N. 1984. Mantle derived Archaean monzodiorites and trachyandesites. *Nature*, **310**:222-224. https://doi.org/10.1038/310222a0

Silva L.C., Armstrong R., Noce C.M., Carneiro M.A., Pimentel M.M., Pedrosa-Soares A.C., Leite C.A., Vieira V.S., Silva M.A., Paes V.J.C., Cardoso-Filho J.M. 2002. Reavaliação da evolução geológica em terrenos pré-cambrianos brasileiros com base em novos dados U-Pb SHRIMP, parte II: Orógeno Araçuaí, Cinturão Mineiro e Cráton São Francisco Meridional. *Revista Brasileira de Geociências*, **32**(4):513-528.

Stern R.A., Hanson G.N. 1991. Archean High-Mg Granodiorite: A Derivative of Light Rare Earth Element-enriched Monzodiorite of Mantle Origin. *Journal of Petrology*, **32**(1):201-238. https://doi.org/10.1093/petrology/32.1.201

Stern R.A., Hanson G.N., Shirey S.B. 1989. Petrogenesis of mantle-derived, LILE-enriched Archean monzodiorites and trachyandesites (sanukitoid rocks) in southwestern Superior Province. *Canadian Journal of Earth Sciences*, **26**(9):1688-1712. https://doi.org/10.1139/e89-145

Sun G., Liu S., Wang M., Bao H., Teng G. 2020. Complex Neoarchean mantle metasomatism: Evidence from sanukitoid diorites-monzodiorites-granodiorites in the northeastern North China Craton. *Precambrian Research*, **342**:105692. https://doi.org/10.1016/j.precamres.2020.105692

Sun S.-S., McDonough W.F. 1989. Chemical and isotopic systematics of oceanic basalts: implications for mantle composition and processes. In: Saunders A.D., Norry M.J. (eds.), *Magmatism in the Ocean Basins*. London: Geological Society of London, p. 313-345. https://doi.org/10.1144/GSL.SP.1989.042.01.19

Tarney J., Jones C.E. 1994. Trace element geochemistry of orogenic igneous rocks and crustal growth models. *Journal of Geological Society*, **151**(5):855-868. https://doi.org/10.1144/gsjgs.151.5.0855

Teixeira W., Ávila C.A., Dussin I.A., Neto A.C., Bongiolo E.M., Santos J.O., Barbosa N.S., 2015. A juvenile accretion episode (2.35–2.32 Ga) in the Mineiro belt and its role to the Minas accretionary orogeny: zircon U–Pb–Hf and geochemical evidences. *Precambrian Research*, **256**:148-169. https://doi.org/10.1016/j.precamres.2014.11.009

Teixeira W., Oliveira E.P., Marques L.S. 2017. Nature and Evolution of the Archean Crust of the São Francisco Craton. In: Heilbron M., Cordani, U.G., Alkmim F. (eds.). *The São Francisco Craton, Eastern Brazil: Tectonic Genealogy of a Miniature Continent*. Springer, p. 29-56. https://doi.org/10.1007/978-3-319-01715-0_3

Tupinambá M., Heilbron M., Valeriano C., Porto Júnior R., Dios F.B., Machado N., Silva L.G.E., Almeida J.C.H. 2012. Juvenile contribution of the Neoproterozoic Rio Negro Magmatic Arc (Ribeira Belt, Brazil): implications for Western Gondwana amalgamation. *Gondwana Research*, **21**(2-3):422-438. https://doi.org/10.1016/j.gr.2011.05.012

Valeriano C.M., Turbay C.V.G., Bruno H., Simonetti A., Heilbron M., Bersan S.M., Strachan R. 2022. Paleo- and Mesoarchean TTG-sanukitoid to high-K granite cycles in the southern São Francisco craton, SE Brazil. *Geoscience Frontiers*, **13**(5):101372. https://doi.org/10.1016/j.gsf.2022.101372

Zhang C., Liu X., Xiao W., Xu J., Shi Y., Gong X., Hu R., Liu P., Zong Y., Xiao Y., Zhang Z., Li R., Li D. 2021. Geochemistry and Sr–Nd–Hf–Pb isotope systematics of late Carboniferous sanukitoids in northern West Junggar, NW China: Implications for initiation of ridge-subduction. *Gondwana Research*, **99**:204-218. https://doi.org/10.1016/j.gr.2021.07.008

Zhang C., Santosh M., Luo Q., Jiang S., Liu L., Liu D. 2019. Impact of residual zircon on Nd-Hf isotope decoupling during sediment recycling in subduction zone. *Geoscience Frontiers*, **10**(1):241-251. https://doi.org/10.1016/j.gsf.2018.03.015

Zheng Y-F. 2019. Subduction zone geochemistry. *Geoscience Frontiers*, **10**(4):1223-1254. https://doi.org/10.1016/j.gsf.2019.02.003